https://ntrs.nasa.gov/search.jsp?R=19750003135 2020-03-23T03:05:13+00:00Z

The Design of Pumpjets for Hydrodynamic Propulsion

EDGAR P. BRUCE, WALTER S. GEARHART, JOHN R. ROSS, AND ALLEN L. TREASTER[1]

The Pennsylvania State University

This paper illustrates a procedure for use in the design of a wake-adapted pumpjet mounted on the aft end of a body of revolution. To this end, a pumpjet is designed for the Akron airship. The propulsor mass flow is selected to minimize kinetic energy losses through the duct and in the discharge jet. The shaft speed and disk size are selected to satisfy specified limits of cavitation performance and to provide acceptable blade loading. The streamtubes which pass through a propulsor mounted on a tapered afterbody follow essentially conical surfaces. A method is provided for defining these surfaces as a function of shroud geometry, rotor head distribution, and the energy distribution of the ingested mass flow. The three-dimensional effects to which the conical flow subjects the cylindrical blade design sections are described and a technique is presented which permits incorporation of these effects in the blade design procedure.

INTRODUCTION

This paper is written under the assumption that the analysis that is normally exercised in selecting a propulsor, based on consideration of factors such as body geometry, vehicle speed, cavitation performance, torque balance, vehicle stability and control, efficiency, noise, simplicity, and expense of manufacture, has been accomplished and the pumpjet has emerged as the best candidate. Guidance in selecting the proper propulsor for a given application is presented in references 1 and 2.

The term "pumpjet" defines a hydrodynamic propulsor which consists of a rotating vane system operating in an axisymmetric shroud or duct.

---

[1] This work was performed at the Ordnance Research Laboratory, The Pennsylvania State University, under the support of the U.S. Navy, Naval Ordnance Systems Command, NOOO 17-70-C-1407.

However, in addition to the rotating vane system, a stationary vane system is utilized at the exit to permit jet discharge through a nozzle with zero peripheral velocity.

The interest in pumpjets has resulted primarily from efforts to develop propulsor systems for both high-speed surface vehicles and submerged vehicles. The attractiveness of pumpjets for high-speed applications originates from the ability to design the propulsor to operate with velocities of smaller magnitude relative to the rotating vanes than the forward velocity of the propelled body. This feature is achieved by proper selection of rotor disk area and shaft speed with respect to the mass flow and energy input of the propulsor. When the velocities relative to the propulsor blades are reduced to a value below the forward velocity of the propelled body, the blading is less susceptible to the inception of cavitation than the body itself. This reduction in the magnitude of the velocities relative to the rotating blade system can normally be accomplished only if the shaft speed and the meridional flow velocity are both reduced. In most cases, this leads to high-torque propulsors of low shaft speeds.

High-torque, low-rotational-speed propulsors require either a stationary vane system or counterrotating rotors to provide an axial discharge jet. This eliminates the kinetic energy losses that are associated with the high circumferential velocities that would otherwise be dumped overboard in the discharge jet.

The original efforts in the design and development of pumpjets are summarized in reference 3. Much of this design philosophy is still used; however, it is the intent of this paper to present an approach that incorporates the results of recent cascade work and includes some of the techniques presently used in axial flow compressor design. This method permits the sizing and design of a pumpjet to satisfy specified performance criteria relating to (1) vehicle forward velocity, (2) available power for propulsion, (3) propulsor shaft speed, (4) vehicle size and shape, and (5) required submergence depth below which no cavitation is tolerable.

To this end, the proper mass flow through the pumpjet to provide a maximum propulsive efficiency must be determined. Once the optimum mass flow has been derived, it is necessary to determine the disk area, blade solidity, and shaft speed which will permit the design of a vane system that satisfies specified limits of resistance to flow separation and cavitation.

On completing the preliminary sizing of the propulsor, a detailed analysis of the flow properties at various stations through the pumpjet must be performed to permit the graphical design of the individual rotor and stator blade systems.

The following paragraphs outline a procedure, summarized above, which has been used with success in the design of pumpjet propulsors. Without reservation, the authors are fully aware of their indebtedness to

past developments at various hydrodynamic and aerodynamic laboratories which provide a part of the basis for the design procedures presented. However, familiarity inevitably supports a tendency to emphasize one's own work. Apologies are offered for any such offense.

Vehicle Boundary Layer Velocity Profile and Drag Coefficient

The propulsor configuration and its performance are highly dependent on the hydrodynamic characteristics of the body or vehicle to which it is to be applied. Under ideal conditions, the inflow velocity to the propulsor would be uniform in the radial and circumferential directions. However, in most cases, energy distortions are present in the ingested flow due to the skin friction drag of the vehicle and/or to wakes from upstream appendages such as shroud support struts, control and stabilizing surfaces, etc.

The circumferential distortions due to upstream appendages can amount to as much as 15 percent of the free-stream velocity and are undesirable when it is considered that vane systems rotating in a circumferentially nonuniform velocity field are prone to periodic cavitation, vibration, and loss of efficiency. For these reasons, every effort should be made to minimize such distortions or mix them out prior to their arrival at the rotating vane system.

Analytical predictions of the velocity profiles near the aft end of a body of revolution are difficult to obtain since the afterbody curvature often produces a pressure gradient normal to the flow that is of the same magnitude as the gradient parallel to the flow. In many cases, existing experimental results for similar bodies can be used and corrected for variations in Reynolds number. It is often far more expedient and reliable to fabricate a scale model and obtain the necessary energy distributions and vehicle drag by either wind or water tunnel tests. A method for estimating the drag of hydrodynamic bodies is given in reference 4 and a method for estimating the velocity profile near the aft end of a body is given in reference 5.

For the illustrative purpose of this paper, a wake-adapted pumpjet has been designed for the U.S. airship Akron. Table I presents the body coordinates of the Akron and the revised coordinates used in this design exercise. Note that the only difference is over the aft 20 percent of the body length, where the contour has been altered slightly to accommodate the pumpjet installation. The necessary velocity and pressure distribution data have been taken from reference 6 which contains the results of a detailed wind tunnel test program conducted on the Akron by the NACA.

To determine the optimum mass flow with respect to minimizing kinetic energy losses dumped overboard in the discharge jet, a reference station is selected near the aft end of the body where the static pressure on

TABLE I.—*Body Coordinates for the Airship Akron and for the Akron Body Modified for Pumpjet Installation*

Percent length	Body radius-to-length ratio	
	Airship Akron	Modified body
0	0	0
1	0.0090	0.0090
2	0.0210	0.0210
3	0.0297	0.0297
4	0.0367	0.0367
5	0.0423	0.0423
6	0.0470	0.0470
7	0.0508	0.0508
10	0.0603	0.0603
15	0.0707	0.0707
20	0.0781	0.0781
25	0.0812	0.0812
30	0.0833	0.0833
35	0.0843	0.0843
40	0.0845	0.0845
45	0.0845	0.0845
50	0.0841	0.0841
55	0.0832	0.0832
60	0.0812	0.0812
65	0.0784	0.0784
70	0.0743	0.0743
75	0.0686	0.0686
80	0.0613	0.0612
85	0.0522	0.0519
90	0.0408	0.0380
95	0.0277	0.0227
99.5	0.00308	0.0117
100	0	0

the hull is equal to its value in the free stream. In addition, it is assumed that the static pressure is constant through the boundary layer at this station. This assumption is valid since the analytically determined static pressure profile at this station, including streamline curvature effects, shows only a very slight variation of static pressure with distance from the body. The velocity profile that exists at the reference station and other bare-body characteristics are shown in figure 1. It is also necessary to estimate the total drag of the vehicle, which includes bare-body drag

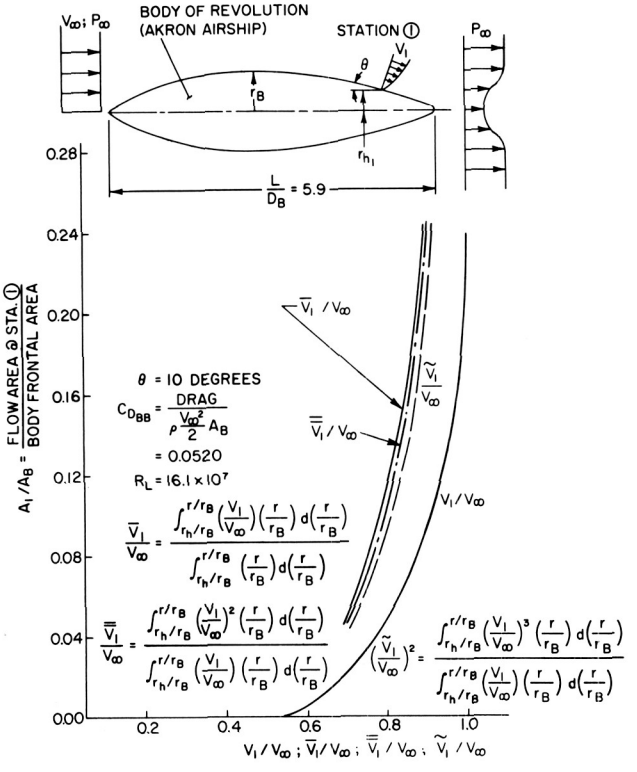

FIGURE 1.—*Velocity distributions associated with the Akron.*

plus increments due to the nacelle or shroud and control surfaces. Reference 4 provides data which is of assistance in estimating the drag increment associated with the control system. In this design example, the added drag due to control surfaces is predicted to be 6 percent of the bare-body drag.

The increment of drag attributed to the frictional effects of the shroud varies with shroud size. This effect can be estimated by referring to figure 2 and noting that, by continuity,

$$A_1\overline{V_1} = A_2\overline{V_2}$$

or

$$r_{T_2} = \left\{\left[\frac{\overline{V_1}}{\overline{\overline{V_2}}}\left(r_{\psi_1}^2 - r_{H_1}^2\right)\right] + r_{H_2}^2\right\}^{1/2} \tag{1}$$

If the wetted surface area of the shroud is approximated by

$$A_s = 4\pi r_{T_2} l_s \tag{2}$$

then the nondimensional shroud drag can be written as

$$C_{D_s} = C_{D_s}' \frac{A_s}{A_B} \tag{3}$$

where C_{D_s}' is the skin friction drag coefficient based on shroud wetted surface area. After substituting equations (1) and (2) into equation (3) and adding the increments due to bare-body and control surface drag, the total thrust coefficient may be expressed as

$$C_T = C_{D_{BB}} + 0.06 C_{D_{BB}} + 4 C_{D_s}' \frac{l_s}{r_B} \left\{ \frac{\overline{V_1}}{\overline{V_2}} \left[\left(\frac{r_{\psi_1}}{r_B} \right)^2 - \left(\frac{r_{H_1}}{r_B} \right)^2 \right] + \left(\frac{r_{H_2}}{r_B} \right)^2 \right\}^{1/2} \tag{4}$$

In equation (4), preliminary values are now assigned to selected quantities as follows: $l_s/r_B = 1.00$; $r_{H_2}/r_B = 0.25$; $\overline{V_1}/\overline{V_2} = 1.15$; and $C_{D_s}' = 0.003$. The accuracy of the estimated values of these quantities will become evident from later developments. It is important to note that the above relation reflects an increase in shroud drag as ingested mass flow increases.

In this estimate, only the frictional drag of the propulsor shroud has been considered. However, it must be remembered that the pressure drag of the body, which was initially included in the bare-body drag coefficient, is substantially reduced by the addition of the propulsor. Thus, the inclusion of the full bare-body drag in all calculations tends to compensate for increases in the form drag of the pumpjet shroud.

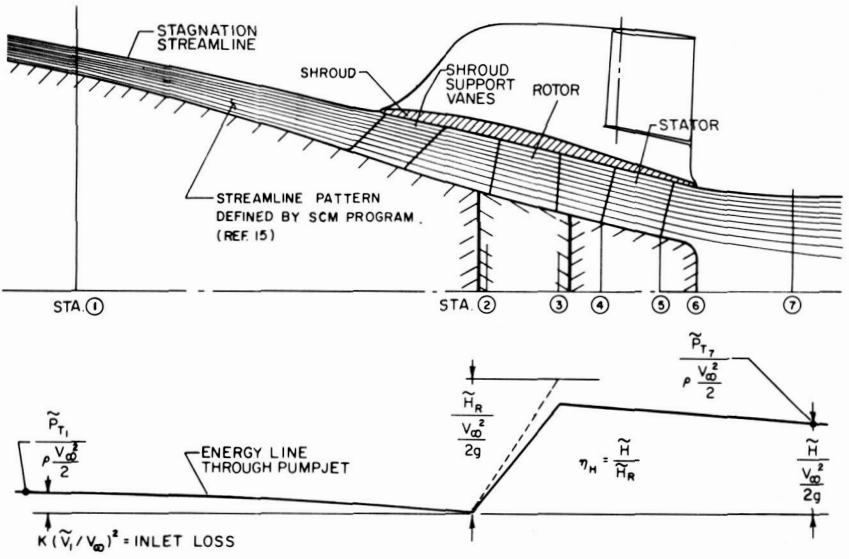

FIGURE 2.—*Streamlines and energy line through the pumpjet.*

Optimum Propulsor Mass Flow

When seeking an engineering design solution involving boundary-layer ingested flow, it is necessary to define three separate average velocity quantities which are a function of the boundary-layer shape at the reference station. These mean quantities are representative of the mass flow rate, the momentum, and the kinetic energy of the ingested flow. For cases where all streamlines are approximately parallel to the body surface, they are defined as follows:

$$\frac{\overline{V_1}}{V_\infty} = \frac{\int_{r_H/r_B}^{r/r_B} \frac{V_1}{V_\infty} \frac{r}{r_B} d\left(\frac{r}{r_B}\right)}{\int_{r_H/r_B}^{r/r_B} \frac{r}{r_B} d\left(\frac{r}{r_B}\right)} \tag{5}$$

$$\frac{\overline{\overline{V_1}}}{V_\infty} = \frac{\int_{r_H/r_B}^{r/r_B} \left(\frac{V_1}{V_\infty}\right)^2 \frac{r}{r_B} d\left(\frac{r}{r_B}\right)}{\int_{r_H/r_B}^{r/r_B} \frac{V_1}{V_\infty} \frac{r}{r_B} d\left(\frac{r}{r_B}\right)} \tag{6}$$

$$\left(\frac{\tilde{V}_1}{V_\infty}\right)^2 = \frac{\int_{r_H/r_B}^{r/r_B} \left(\frac{V_1}{V_\infty}\right)^3 \frac{r}{r_B} d\left(\frac{r}{r_B}\right)}{\int_{r_H/r_B}^{r/r_B} \frac{V_1}{V_\infty} \frac{r}{r_B} d\left(\frac{r}{r_B}\right)} \tag{7}$$

For many cases, the three values given by the different definitions for the mean velocity will not differ significantly. However, the individual values are dependent on the "shape factor" of the boundary layer and for boundary-layer profiles having a ratio of displacement to momentum thickness of 1.5 or greater it is important to insert the respective values in mass flow, momentum, or energy relations. This practice will be followed in this paper even though the velocities, as defined by equations (5), (6), and (7) and plotted in figure 1, indicate little difference.

Propulsion devices depend on the principle of reaction. The impulse-momentum relation when applied in the axial direction between Stations ① and ⑦ of figure 2, where it is assumed that free-stream static pressure exists, results in

$$T = \rho A_1 \overline{\overline{V}}_1 (\Delta \overline{\overline{V}}_a) \tag{8}$$

where $\Delta\overline{\overline{V}}_a$ is the average change in axial velocity. This expression can be written in terms of the thrust coefficient as

$$C_T = 2\frac{A_1}{A_B}\frac{\overline{\overline{V}}_1}{V_\infty}\frac{\Delta\overline{\overline{V}}_a}{V_\infty} \tag{9}$$

Referring to equation (9), the product $(A_1/A_B)(\overline{\overline{V}}_1/V_\infty)$ represents the nondimensionalized mass flow rate through the pumpjet and the quantity $\Delta\overline{\overline{V}}_a/V_\infty$ represents the axial acceleration of the fluid between Stations ① and ⑦. It is evident that to obtain a given thrust, the product of these two quantities must remain constant. This can be achieved with significant variations in the individual values of the mass flow rate and the acceleration. The criterion used in selecting the proper mass flow rate is based on minimizing the energy dumped overboard in the discharge jet and the energy losses in the duct inlet. The parameter normally used in defining this performance criterion is termed the propulsive coefficient (sometimes referred to as propulsive efficiency). It expresses the relative effectiveness of converting the energy placed in the fluid by the propulsor into propulsive vehicle energy. Since the propulsor is ingesting low-energy boundary-layer fluid, the selection of the optimum mass flow rate is influenced by the shape and energy of the velocity profile near the aft end of the body as discussed in references 2, 7, and 8.

The approach which is used to determine the optimum mass flow rate is based on analysis of averaged energy relations through the pumpjet, thereby eliminating the need for defining the propulsive vehicle energy. This quantity is confusing because its definition often leads to propulsive coefficients greater than unity. Referring to figure 2, the energy relation between Stations ① and ⑦ can be written

$$\tilde{P}_{T_1} = \tilde{P}_{T_7} - \gamma\tilde{H} + K\rho\frac{\tilde{V}_1^2}{2} \tag{10}$$

This relation is depicted graphically in figure 2. Assuming the same static pressure at both stations, the nondimensional relation defining the energy placed in the fluid can be expressed as

$$\frac{\tilde{H}}{(V_\infty^2/2g)} = \left(\frac{\tilde{V}_7}{V_\infty}\right)^2 - \left(\frac{\tilde{V}_1}{V_\infty}\right)^2 + K\left(\frac{\tilde{V}_1}{V_\infty}\right)^2$$

Since $\tilde{V}_7$ can be closely approximated by $\tilde{V}_1 + \Delta\overline{\overline{V}}_m$, this expression reduces to

$$\frac{\tilde{H}}{(V_\infty^2/2g)} = 2\frac{\Delta\overline{\overline{V}}_m}{V_\infty}\frac{\tilde{V}_1}{V_\infty} + \left(\frac{\Delta\overline{\overline{V}}_m}{V_\infty}\right)^2 + K\left(\frac{\tilde{V}_1}{V_\infty}\right)^2 \tag{11}$$

where $\Delta\overline{\overline{V}}_m/V_\infty$ is obtained from equations (4) and (9) with consideration

of the local body geometry. The variation of $\Delta\bar{\bar{V}}_m/V_\infty$ with amount of ingested mass flow is shown in figure 3. The last term in equation (11) represents the energy loss in the shroud inlet. A typical value of the loss coefficient for this type of inlet, $K=0.13$, was used in this case.

The hydraulic efficiency of a turbomachine is defined as the ratio of the energy placed in the fluid to the shaft energy. The energy placed in the fluid could be determined from an averaged total head traverse fore and aft of the rotor-stator system and the shaft energy could be determined from the shaft speed and torque. Over the range of flows to be investigated here, it has been assumed that the hydraulic efficiency, defined by the ratio

$$\eta_H = \frac{\tilde{H}}{\tilde{H}_R} \tag{12}$$

remains constant at 0.89, a value typical of axial-flow pumps. This estimate of the hydraulic efficiency can be evaluated later in the design exercise by using the final spanwise loading and flow characteristics and the technique described in reference 9.

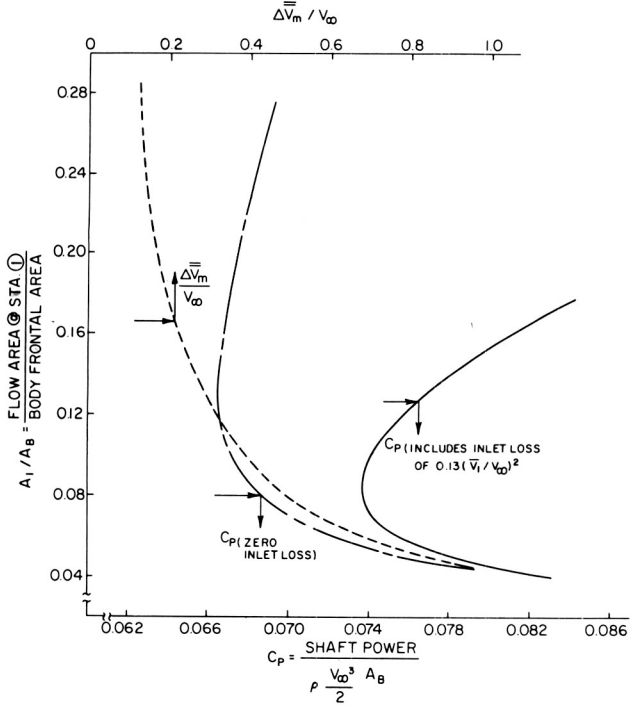

FIGURE 3.—*Power requirements and meridional velocity change as a function of flow area at Station 1.*

A nondimensional shaft power coefficient can now be defined.

$$C_P = \frac{P}{\frac{1}{2}\rho V_\infty^3 A_B} = \frac{\tilde{H}_R}{(V_\infty^2/2g)} \tilde{C}_m \tag{13a}$$

where

$$\tilde{C}_m = \frac{A_1}{A_B} \frac{\tilde{V}_1}{V_\infty} \tag{13b}$$

Substituting equations (11), (12), and (13*b*) in equation (13*a*) gives

$$C_P = \frac{1}{\eta_H} \left[2 \frac{\Delta\overline{\overline{V}}_m}{V_\infty} \frac{\tilde{V}_1}{V_\infty} + \left(\frac{\Delta\overline{\overline{V}}_m}{V_\infty} \right)^2 + K \left(\frac{\tilde{V}_1}{V_\infty} \right)^2 \right] \frac{A_1}{A_B} \frac{\tilde{V}_1}{V_\infty} \tag{14}$$

By substituting the velocity ratios at given values of A_1/A_B as indicated by figure 1, a plot of the shaft power coefficient can be obtained as shown in figure 3. The optimum mass flow with respect to minimizing required shaft power corresponds to $A_1/A_B = 0.10$, $\tilde{V}_1/V_\infty = 0.78$, and $\Delta\overline{\overline{V}}_m/V_\infty = 0.39$. The optimum was chosen slightly above the predicted value to ensure staying above that portion of the power curve where adverse C_P gradients occur.

The magnitude by which the inlet loss affects the performance of the propulsor is illustrated in figure 3 by the plot of the power coefficient associated with zero inlet loss. The advantage of boundary-layer intake for this propulsor configuration should also be emphasized. The increased performance associated with boundary-layer intake can be illustrated by considering an alternate propulsor configuration that is strut-mounted at a distance from the hull sufficient to permit ingesting fluid of free-stream dynamic energy. The power required for this configuration is found by substituting $\tilde{V}_1/V_\infty = 1$ into the previous equations and is 15-percent greater than that associated with the propulsor that takes advantage of boundary-layer intake.

CAVITATION PERFORMANCE

The problem of propulsor cavitation is largely dependent on the degree to which cavitation has to be avoided. It has been well established that limited cavitation occurring within the blade passages of pumps, propellers, or pumpjets does not affect the propulsor performance or efficiency. However, strongly developed cavitation can lead to complete performance breakdown and falloff in shaft torque. The problem of cavitation is considerably complicated when it is necessary to avoid local, incipient

cavitation at specified vehicle speeds and depths. In this case, the propulsor must operate with a minimum of cavitation-induced noise, vibration, and erosion, all of which can be introduced with only minute sporadic cavitation.

The parameter used to describe the cavitation performance of pumping machinery is suction specific speed. An analogous parameter, which has been used by various hydrodynamic laboratories, is termed a cavitation index. The use of the latter cavitation parameter permits describing the cavitation performance of either a rotating or stationary element of the hydrodynamic machine. The suction specific speed parameter, by definition, involves a shaft speed and has generally been used to describe the overall cavitation performance of the entire shrouded rotor-stator system. A discussion indicating the relation of these two cavitation parameters is found in reference 3.

The cavitation index will be used in this paper as the cavitation performance parameter. It is defined as the ratio of the difference between the ambient static pressure at the centerline of the vehicle and the vapor pressure to the dynamic head of the free-stream fluid as shown below.

$$\sigma=\frac{h_{\text{sub}}+h_{\text{atm}}-h_V}{(V_\infty{}^2/2g)}=\frac{h_{\text{sub}}+32.0}{(V_\infty{}^2/2g)}=\frac{p_\infty-p_V}{\frac{1}{2}\rho V_\infty{}^2} \tag{15}$$

The critical cavitation index, σ_{cr}, relates the unique conditions of depth and forward velocity at which cavitation inception occurs. Referring to figure 2, the energy relation expressed between Stations ① and ② has the form:

$$\frac{p_2-p_\infty}{\frac{1}{2}\rho V_\infty{}^2}=\left(\frac{\tilde{V}_1}{V_\infty}\right)^2-\left(\frac{\tilde{V}_2}{V_\infty}\right)^2-0.13\left(\frac{\tilde{V}_1}{V_\infty}\right)^2 \tag{16}$$

The minimum pressure coefficient along the blade profile at the tip can be defined as

$$C_b=\frac{p_2-p_{\text{min}}}{\frac{1}{2}\rho W_2{}^2} \tag{17}$$

The relative velocity, W_2, at the rotor blade tip is used in this relation since the velocity at the tip is a maximum, making this region most critical with respect to cavitation.

By utilizing equations (15), (16), and (17) and letting p_{min} equal the vapor pressure of the fluid, the following relation defining the critical cavitation index is obtained.

$$\sigma_{\text{cr}}=C_b\left(\frac{W_2}{V_\infty}\right)^2-\left(\frac{\tilde{V}_1}{V_\infty}\right)^2+\left(\frac{\tilde{V}_2}{V_\infty}\right)^2+0.13\left(\frac{\tilde{V}_1}{V_\infty}\right)^2 \tag{18}$$

The average values of the quantities indicated in equation (18) will be used to obtain values of cavitation performance for preliminary selection of disk area and shaft speed. On this basis, with

$$\frac{\tilde{V}_2}{V_\infty}=\frac{\tilde{V}_1}{V_\infty}\frac{A_1}{A_2} \tag{19a}$$

and with

$$\left(\frac{W_2}{V_\infty}\right)^2=\left(\frac{\tilde{V}_2}{V_\infty}\right)^2+\left(\frac{U_T}{V_\infty}\right)^2 \tag{19b}$$

we have

$$\sigma_{cr}=C_b\left[\left(\frac{\tilde{V}_1}{V_\infty}\right)^2\left(\frac{A_1}{A_2}\right)^2+\left(\frac{U_T}{V_\infty}\right)^2\right]+\left(\frac{\tilde{V}_1}{V_\infty}\right)^2\left(\frac{A_1}{A_2}\right)^2-0.87\left(\frac{\tilde{V}_1}{V_\infty}\right)^2 \tag{20}$$

This relationship can be expressed nondimensionally in terms of the advance ratio, rotor hub and tip radii, and mass flow rate coefficient by noting that

$$J=\frac{V_\infty}{nD_B} \tag{21a}$$

$$\frac{U_T}{V_\infty}=\frac{\pi}{J}\frac{r_T}{r_B} \tag{21b}$$

$$\frac{A_2}{A_B}=\frac{(r_T/r_B)^2-(r_H/r_B)^2}{\cos\theta} \tag{21c}$$

By inserting these expressions and equation (13*b*) into equation (20), a very useful relation is obtained that permits the selection of values of disk area and advance ratio which satisfy specified limits of cavitation performance.

$$\sigma_{cr}=C_b\left\{\tilde{C}_m{}^2\left[\frac{\cos\theta}{(r_T/r_B)^2-(r_H/r_B)^2}\right]^2+\left(\frac{\pi}{J}\right)^2\left(\frac{r_T}{r_B}\right)^2\right\}$$

$$+\tilde{C}_m{}^2\left\{\left[\frac{\cos\theta}{(r_T/r_B)^2-(r_H/r_B)^2}\right]^2-0.87\left(\frac{A_B}{A_1}\right)^2\right\} \tag{22}$$

To illustrate the use of equation (22), it has been solved as a function of r_T/r_B for various advance ratios by substituting the quantities $\tilde{C}_m=0.078$, $A_1/A_B=0.100$, and $\tilde{V}_1/V_\infty=0.780$ obtained from optimum conditions indicated by solution of equation (14). The tip section minimum pressure coefficient C_b was set equal to 0.3, which is representative

for thin airfoil sections at zero incidence. The quantity r_H/r_B is, in most cases, dictated by the geometry of the tail-cone and limited by the mechanical design of the aft bearings and shafting. In this case, r_H/r_B was taken equal to 0.25. The angle θ, which is also specified by the tail-cone geometry as shown in figure 1, was equal to 13° in this case. The results of substituting these values for the various parameters into equation (22) are plotted in figure 4. The curves indicate that, for a given disk area, as advance ratio is increased (shaft speed decreased) the cavitation performance improves. Conversely, for a given advance ratio, as the disk area is increased (or as greater diffusion of the flow is permitted between Stations ① and ②), the cavitation index also improves. However, efficient operation over the complete range of these two design variables is not possible since extremely low shaft speeds require such high blade loadings that flow separation will occur on the blades themselves. By the same reasoning, the flow from Station ① to Station ② can be decelerated only a certain amount before separation on the hull can be expected. For these reasons, the disk area and advance ratio indicated as the design point in figure 4 were selected for this design exercise. At this point, there is approximately 15-percent diffusion of the flow between Stations ① and ②. Little is gained in terms of increased cavitation performance by further diffusion since the curve is starting to obtain a gradual slope. In

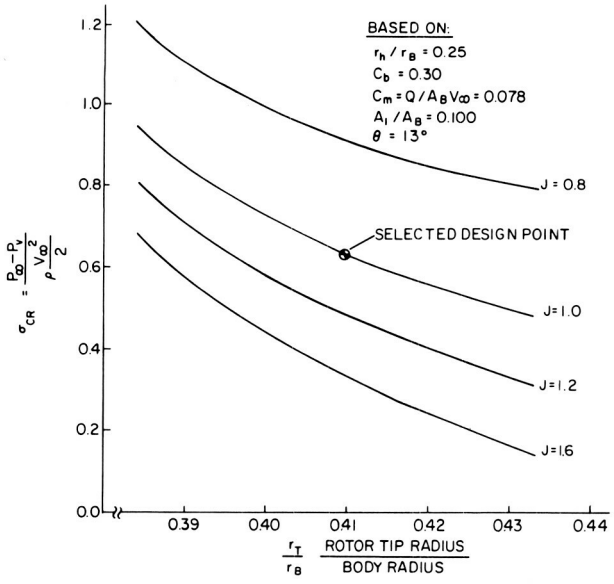

FIGURE 4.—*Critical cavitation index as a function of rotor tip radius and advance ratio.*

addition, this amount of diffusion does not significantly risk flow separation on the hull. It is recommended that the sizing of the shroud inlet be based on the studies of reference 10 which indicate the amount of prediffusion that can be obtained efficiently with nonuniform energy flows. This approach provides a preliminary estimate of disk size. A more detailed evaluation of the flow properties at Station ②, obtained from a computerized solution of the flow field within the duct, will be presented later.

To proceed with the design example, it is now assumed that operational conditions require a forward speed of 50 knots at a cavitation-free depth of 40 feet. It is also assumed that the shaft speed is unrestricted and can be selected at the designer's discretion. Using the relation given as equation (15), it is found that these conditions correspond to a critical cavitation index of 0.650. Referring to figure 4 shows that this value of cavitation index is compatible with the values of r_T/r_B and J selected previously. The predicted cavitation performance is approximate since average values of velocities were used; however, it is representative and final predictions cannot be made until the blade sections are designed. The blade design procedure and the resulting critical cavitation indices are presented in a later section.

It must be emphasized that the preceding design considerations have been directed toward predicting the onset of blade surface cavitation. A second form of cavitation occurs in shrouded propulsors due to the presence of secondary flows such as tip clearance leakage flow. This flow generates cavitation in the clearance gap itself. After proceeding through the gap, this fluid rolls up into a tip vortex of low core pressure. The leakage flow also impinges on the tip of the stator system, causing periodic cavitation. It is usual in pumpjets to find that the cavitation resulting from secondary flows occurs before blade surface cavitation. However, research described in references 11, 12, and 13 provides design criteria which, if properly applied, will give overall propulsor cavitation performance within the limits previously described.

Blade Geometry and Loading Distribution

Satisfying the cavitation requirements of the blading does not imply that flow separation will not occur from excessive blade loading, especially near the root section where relative flow velocities are low. Flow separation leads to high energy losses and creates large wakes which promote both cavitation and vibration.

The magnitude of the average rotor head $\tilde{H}_R/(V_\infty^2/2g)$ was evaluated previously using equations (11) and (12). It is now necessary to obtain a radial distribution of this rotor head which also satisfies established limits of blade loading.

By Euler's equation, the rotor head can be equated to the mass averaged integrated value at the rotor exit, assuming that there is no peripheral velocity component in the flow at the rotor inlet.

$$\frac{\tilde{H}_R}{\frac{V_\infty^2}{2g}} = 2 \frac{\int_{r_H/r_B}^{r_T/r_B} \frac{V_{m_3}}{V_\infty} \frac{U}{V_\infty} \frac{V_{\theta_3}}{V_\infty} \frac{r}{r_B} d\left(\frac{r}{r_B}\right)}{\int_{r_H/r_B}^{r_T/r_B} \frac{V_{m_3}}{V_\infty} \frac{r}{r_B} d\left(\frac{r}{r_B}\right)} \tag{23}$$

The selection of the radial distribution of V_{θ_3}/V_∞ requires an iterative procedure since many distributions would satisfy this condition, including the free vortex distribution shown in figure 5. However, near the hub the free vortex loading requires, in many cases, an absolute peripheral component of velocity greater than the peripheral wheel speed. This is undesirable since turning the relative flow past the axial direction is not recommended for reasons of separation (see ref. 14). The free vortex loading is also undesirable since kinetic energy losses are minimized in a discharge jet whose velocity is uniform and approaches the vehicle velocity in magnitude. A uniform discharge jet cannot be obtained with free vortex loading since boundary layer fluid is ingested. This condition can be more closely approached with a forced vortex loading. The forced vortex V_{θ_3}/V_∞ distribution shown in figure 5 was selected after several iterations and was used as input to the Streamline Curvature Method

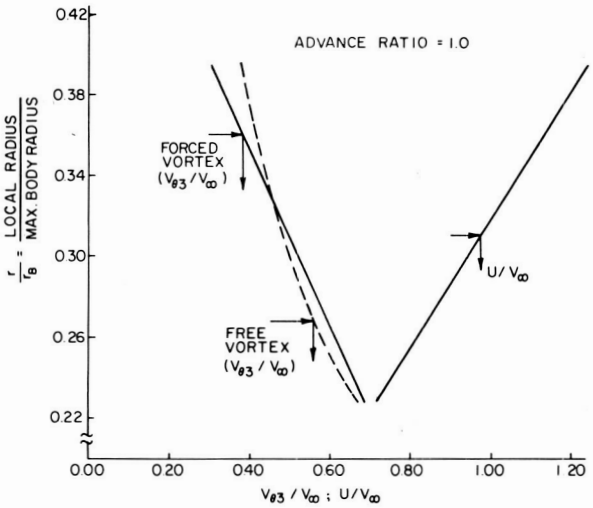

FIGURE 5.—*Rotor velocity and load distribution.*

(SCM) computer program of reference 15. This program provides a solution to the axisymmetric flow field from which the detailed flow properties at various stations through the pumpjet can be obtained. A general discussion of a computerized version of this method, its operation and application, is presented in Appendix I. To obtain a solution, the coordinates of the vehicle hull are used as input and are spline fit to describe the inner contour of the pumpjet. The outer contour is defined by passing a spline curve through points corresponding to the coordinates of the stagnation streamline at Station ①, the shroud inlet, the rotor tip, and the shroud exit. The shroud exit is sized to reflect the "vena contracta" of the discharge jet as discussed in reference 16. This geometric information, in addition to the energy and velocity profiles at Station ① and the radial distribution of rotor head at Station ③, is the information required as program input data.

The velocity and energy profiles obtained as SCM program output at the rotor inlet and exit and at the stator inlet and exit are shown in figures 6 and 7. Using these velocity distributions and an established separation criterion such as the Diffusion Factor described in reference 17, the blade solidity necessary to prevent separation can be obtained. The diffusion factor, D, is defined below for rotor blades. For trailing edge loaded blades it is suggested that a value of 0.5 or less be maintained.

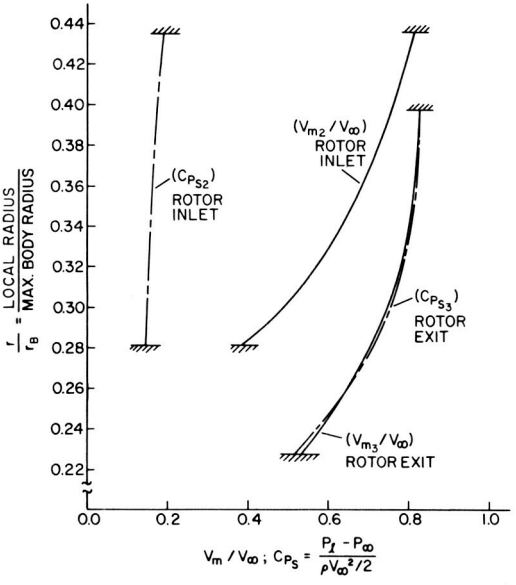

FIGURE 6.—*Velocity and static energy profiles at rotor inlet and exit.*

$$D=1+\frac{1}{2}\frac{V_{\theta_3}}{W_2}\frac{t}{c}-\frac{W_3}{W_2} \tag{24}$$

For preliminary design, the length of the chord can be computed from the projected view of the blade system shown by figure 2 and the vector mean of the velocities relative to the blade at inlet and exit. The diffusion factor and lift coefficient are plotted in figure 8 as a function of r/r_B for a 13-bladed rotor system and a 9-bladed stator system.

Before leaving the discussion regarding the selection of the spanwise loading distribution on the rotor, it must be emphasized that wake-adapted vane systems such as the propeller and pumpjet have an unparalleled potential for the generation of secondary flows. To create secondary flows in blade passages, the primary requirement is an upstream component of vorticity normal to the relative flow at the blade inlet. It is obvious that with boundary-layer intake this condition is amply satisfied and, in contrast to axial-flow compressors where only a fraction of the blade span is subjected to a wall shear flow, the blading of a wake-adapted propulsor is subjected to these flows over the entire blade span. In reference 18, this secondary flow problem has been investigated both analytically and experimentally. Based on this reference, the following physical reasoning is presented with regard to the origin of the secondary flow.

The vane turns the fluid because of the pressure difference between the suction and pressure surfaces. If this pressure differential varies from one

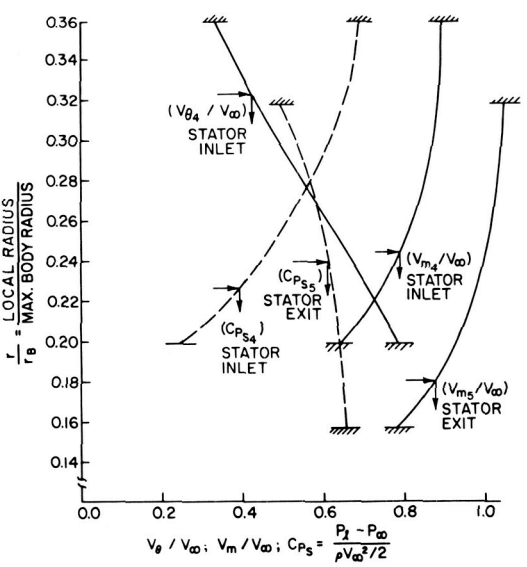

FIGURE 7.—*Velocity and static energy profiles at stator inlet and exit.*

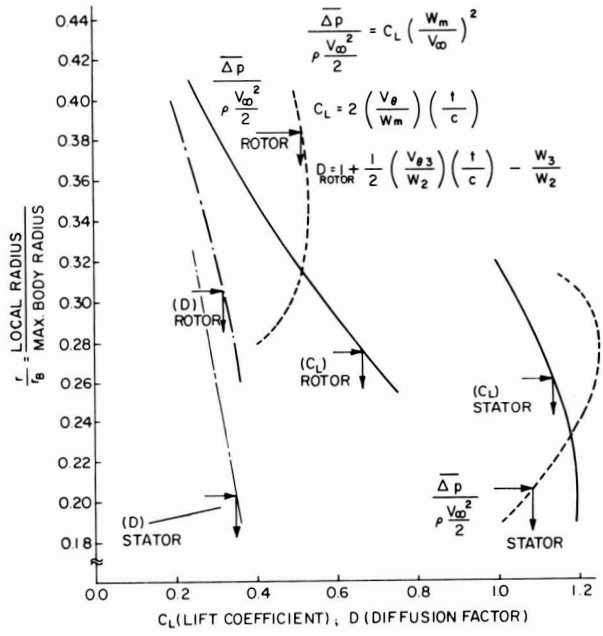

FIGURE 8.—*Spanwise distribution of lift coefficient, diffusion factor, and average pressure differential.*

spanwise location to the next, a spanwise pressure gradient will exist causing spanwise velocities which contribute to the secondary flow. This spanwise pressure gradient is represented by the radial distribution of $\overline{\Delta p}/(\frac{1}{2}\rho V_\infty^2)$ plotted in figure 8. It is obvious that the loading distribution could be improved in the aspect of reducing secondary flows. However, to obtain a uniform radial distribution of average pressure differential requires excessive fluid turning at the rotor hub sections. It is evident from this brief discussion that the relative magnitude of the loss in both efficiency and cavitation performance associated with minimizing secondary flows, avoiding excessive fluid turning, or discharging a jet having relatively high shear and kinetic energy losses must be considered in the selection of the loading distribution.

In summary, this phase of the preliminary design required several iterations to obtain a distribution of rotor head and blade solidity that satisfied propulsive energy requirements and blade cavitation and separation criteria. The blade solidity was chosen somewhat higher than necessary to ensure that the cavitation characteristics of the blading would be more critical with respect to the velocity of the relative flow than the blade loading. In the next section, additional consideration is given to these matters and to the detailed design of typical cylindrical blade sections for the rotor and stator.

MEAN STREAMLINE METHOD OF BLADE DESIGN

The design of blade sections requires the use of a method general enough to accommodate practical applications in which the blade sections are subjected to a flow which, in most cases, is not two dimensional. Most available methods contain a high degree of mathematical and computational complexity and, therefore, require a lengthy period of detailed study before they can be applied successfully. It appears to be impossible for the average designer to become familiar with a sufficient number of methods to be able to correct and modify the two-dimensional solutions to reflect the typical three-dimensional flows normally encountered. Even when automatic computation is used and programs are available, the designer must have a full understanding of the method of solution used.

Consequently, it is desirable for a designer to be familiar with a method that is not too complicated but which is still generally applicable. On this basis, the mean streamline method of reference 14 has been used at the Ordnance Research Laboratory for the blade design of a number of axial-flow pumps. This method of blade design, applicable to the indirect problem, has several very attractive features. Among the most important are

(1) It permits the designer to derive a blade shape of arbitrary thickness and chordwise loading distribution while providing a specified amount of fluid turning.

(2) It provides the capability to account for three-dimensional flow effects, such as changes in the axial velocity along the blade chord and changes in total energy relative to the blade row from leading edge to trailing edge.

Evaluations of the performance of axial-flow pumpjet designs, as determined in wind tunnel and water tunnel tests at the Ordnance Research Laboratory, have indicated values of blade thickness and loading distributions with satisfactory resistance to cavitation. The loading distribution clearly shows characteristics prevalent with trailing edge loaded blades, while the thickness distribution shows that the leading edge as well as the trailing edge should be kept thin. The thin forward portion of the blade, in conjunction with the loading distribution described above, desirably reduces the local blade surface velocities in the vicinity of the leading edge. This is important since this is the region that is most susceptible to the inception of cavitation.

As an illustration of the application of the mean streamline method of blade design, rotor and stator cylindrical blade sections have been designed for the Akron pumpjet at values of r/r_B equal to 0.345 and 0.265, respectively. These blade sections are located near the midspan position of each blade system.

The basic input data required to initiate the blade design procedure are the vehicle geometry and the flow properties at the rotor and stator inlet and exit stations. The change in the flow properties across a single element of the propulsor—for example, the rotor—is related to the average pressure change across the element by the impulse-momentum relation. Figure 9 depicts the basic geometric characteristics, velocity components, and flow directions for a rotor blade cylindrical section of axial length l located at a distance r from the centerline of a vehicle of maximum radius r_B. The meridional and peripheral velocity components at the inlet and exit stations are V_{m_2}, and V_{m_3} and V_{θ_3}, respectively. Due to the taper of the body and the effect of the rotor, the streamline that enters the rotor at the radius r exits from the rotor at a radius less than r. The manner in which this nonaxial character of the flow influences the blade design procedure is described in the paragraphs that follow.

The development of a portion of the cylindrical section of radius r and thickness Δr is shown in figure 10. The rotation of the rotor at the angular velocity ω gives rise to the blade peripheral velocity, $U = r\omega$, as shown. The average pressure, $\overline{\Delta p}$, represents the uniform pressure which, when applied over the incremental area $l(\Delta r)$ in the time increment Δt produces a change in the peripheral momentum of the flow equal to $m(\Delta V_\theta)$. Thus the

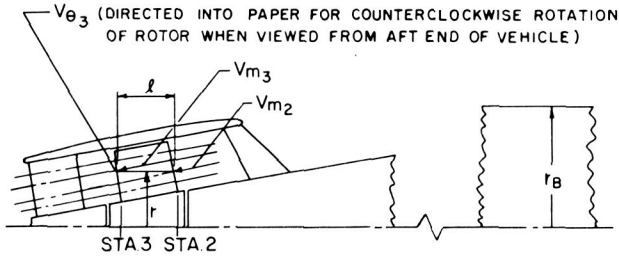

FIGURE 9.—*Basic geometric and flow characteristics.*

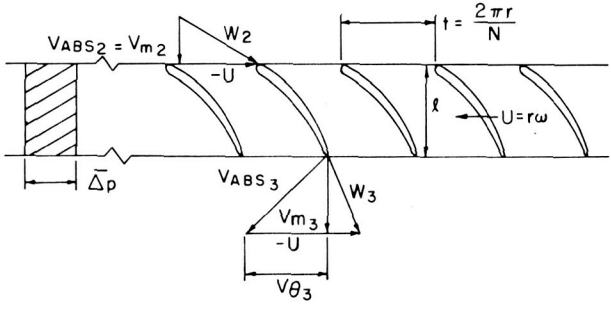

FIGURE 10.—*Rotor cylindrical section development.*

impulse-momentum relation, when applied in the peripheral direction, is

$$F(\Delta t) = m(\Delta V_\theta) \tag{25}$$

where

$$F = N(\overline{\Delta p})l(\Delta r)$$

$$\frac{m}{\Delta t} = 2\pi\rho V_m r(\Delta r)$$

$$\Delta V_\theta = V_{\theta_3} - V_{\theta_2}$$

Combining these with $V_m = \frac{1}{2}(V_{m_2} + V_{m_3})$ and $V_{\theta_2} = 0$ leads to the relation

$$\overline{\Delta p} = \frac{\pi\rho r}{Nl}(V_{m_2} + V_{m_3})V_{\theta_3} \tag{26}$$

By dividing this expression by the quantity $\frac{1}{2}\rho V_\infty^2$, the useful nondimensional expression presented as equation (27) is obtained.

$$\frac{\overline{\Delta p}}{\frac{1}{2}\rho V_\infty^2} = \frac{2\pi r_B}{Nl}\left(\frac{V_{m_2}}{V_\infty} + \frac{V_{m_3}}{V_\infty}\right)\frac{V_{\theta_3}}{V_\infty}\frac{r}{r_B} \tag{27}$$

The uniform pressure $\overline{\Delta p}$ is related to the actual axial pressure distribution $\Delta p = \Delta p(l')$ by the expression

$$\overline{\Delta p} = \frac{1}{l}\int_0^l \Delta p(l')\, d(l') \tag{28}$$

where l' denotes axial position along the rotor cylindrical section. The $\Delta p/(\frac{1}{2}\rho V_\infty^2)$ distributions and the level of the quantity $\Delta p/(\frac{1}{2}\rho V_\infty^2)$ used in the design of the rotor and stator blade sections for the Akron propulsor are shown on the right in figures 11 and 12, respectively.

As defined by equation (27), the average pressure change is proportional to the total change in the peripheral velocity component. For the rotor, the variation of V_θ across the blade section from $V_\theta = 0$ at the inlet to $V_\theta = V_{\theta_3}$ at the exit would be a linear function of l' if $\overline{\Delta p}$ represented the actual loading distribution; i.e., if $\Delta p \neq \Delta p(l')$. However, since this is not the case, it is necessary to relate the variation of V_θ with l' to the variation of Δp with l'. This is achieved by dividing the loading distribution into segments and noting that

$$\left(\frac{V_\theta}{V_\infty}\right)_{l'=al} = \left(\frac{V_{\theta_3}}{V_\infty}\right)_{r_{3_{l'}}/r_B} \frac{\int_0^{l'} \Delta p\, d(l')}{\int_0^l \Delta p\, d(l')} = \left(\frac{V_{\theta_3}}{V_\infty}\right)_{r_{3_{l'}}/r_B} K_{aR} \tag{29}$$

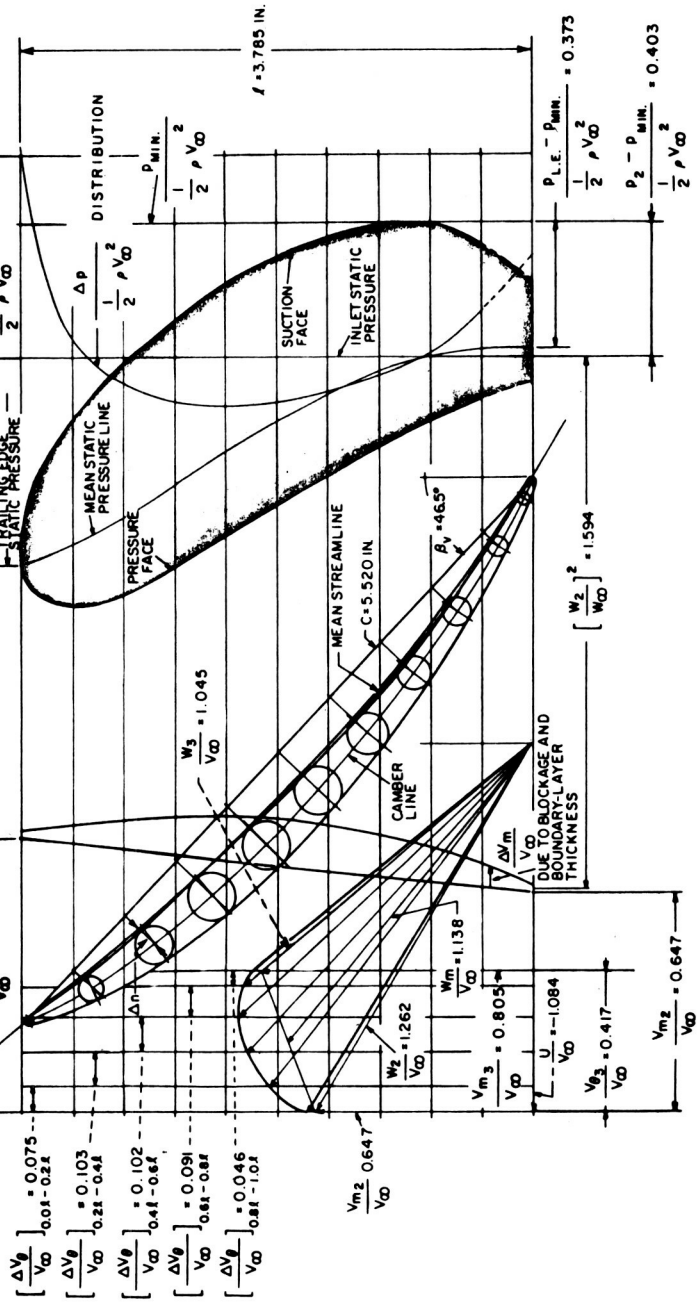

FIGURE 11.—*Rotor cylindrical design section at* $r/r_B = 0.345$.

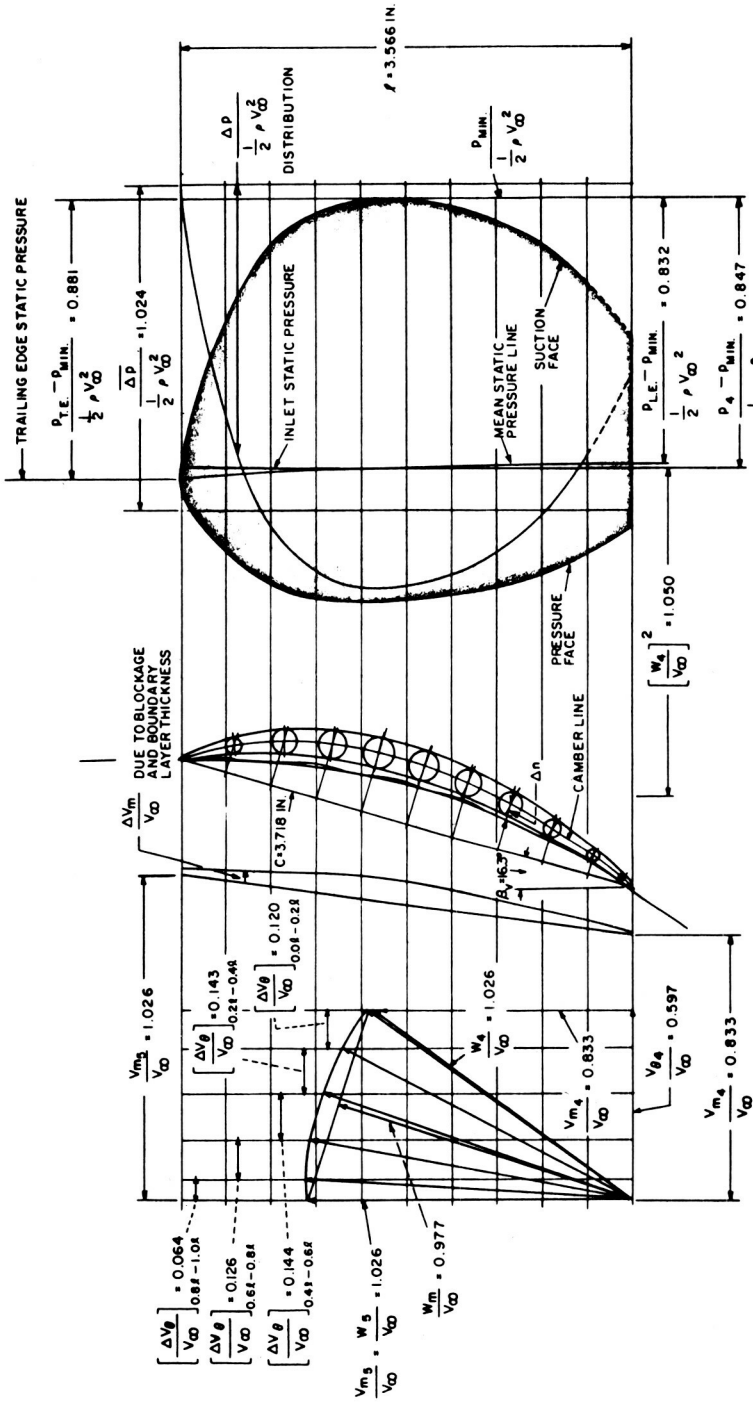

FIGURE 12.—*Stator cylindrical design section at* $r/r_B = 0.265$.

where $a = 0, 0.2, 0.4, \ldots, 1.0$; $(V_{\theta_3}/V_\infty)_{r_{3l'}/r_B}$ is the value of the peripheral velocity at the rotor trailing edge on the streamline that passes through the rotor cylindrical section at l'; and K_{a_R} is a function of l'/l alone for a given loading distribution. The quantity $\int_0^{l'} \Delta p \, d(l')$ represents the area under the Δp versus l' curve between the points 0 and l' and $\int_0^{l} \Delta p \, d(l')$ represents the total area.

It is important to note that equation (29) as written applies to cases in which the propulsor element imparts a peripheral velocity component to flow that had only a meridional component at the inlet. In the case of the stator, the inflow contains both a meridional and a peripheral velocity component. The function of the stator is to reduce the peripheral component to zero at the trailing edge. Thus, for the stator, $K_{a_s} = 1 - K_{a_R}$ where K_{a_R} is the value given by inserting the stator loading distribution and the appropriate values of $(V_{\theta_4}/V_\infty)_{r_{4l'}/r_B}$ into equation (29).

Examination of figures 2 and 9 reveals that the flow streamlines are inclined at an angle to cylindrical blade sections, and reference to figures 5 and 7 reveals that V_θ is a function of r at the rotor exit and at the stator inlet. Consideration of these factors has led to the following procedure for selection of the values of $(V_{\theta_3}/V_\infty)_{r_{3l'}/r_B}$, or $(V_{\theta_4}/V_\infty)_{r_{4l'}/r_B}$, to be used in equation (29). Referring to figure 2, and restricting consideration to the rotor, locate the points $l' = al$ along the line of length l determined by the intersection of the particular rotor cylindrical section under consideration with the plan view of the rotor. Streamlines passing through the points along l denoted by increasing values of l' can then be approximated and the radial position, denoted by $r_{3l'}$, where these streamlines exit from the rotor can be determined. The flow along these streamlines enters the rotor with no peripheral velocity and must exit from the rotor at $r_{3l'}$ with the peripheral velocity $(V_{\theta_3}/V_\infty)_{r_{3l'}/r_B}$ given by entering the V_{θ_3}/V_∞ curve in figure 5 at $r_{3l'}/r_B$. Thus the peripheral velocity at a point l' on a rotor blade cylindrical section is given by the product of the exit peripheral velocity associated with the streamline that intersects the cylindrical section at l' and the fraction of the loading that is concentrated between the leading edge and l'. Similar reasoning, when applied to the stator, leads to the conclusion that the peripheral velocity at a point l' on a stator blade cylindrical section is given by the product of the inlet peripheral velocity associated with the streamline that intersects the cylindrical section at l' and the fraction of the loading that is concentrated between the point l' and the trailing edge.

At this point, it is possible to construct a portion of the relative flow velocity diagrams shown on the left in figures 11 and 12. For the rotor section, with $r/r_B = 0.345$ and $J = 1.0$, $U/V_\infty = 1.084$ by equation (21*b*). From figures 5 and 6, $V_{m_2}/V_\infty = 0.647$, $V_{m_3}/V_\infty = 0.805$, and $V_{\theta_3}/V_\infty = 0.417$. The direction and magnitude of the inlet and exit relative velocity vectors W_2/V_∞ and W_3/V_∞ are given by vector addition of the components

$-U/V_\infty$ and V_{m_2}/V_∞, and $(-U/V_\infty)+(V_{\theta_3}/V_\infty)$ and V_{m_3}/V_∞, respectively. The mean relative velocity vector, W_m/V_∞, is also defined, as described in reference 14, since it terminates on the midpoint of the line connecting the end points of the inlet and exit relative velocity vectors. Application of the technique described above also defines the incremental changes $\Delta V_\theta/V_\infty$ associated with 20-percent length increments along l; thus vertical lines can be constructed based on the magnitude of these increments. If the blade section had no thickness and no boundary layer, the end points of the internal mean flow relative velocity vectors would be defined by the points of intersection of the vertical lines denoting the internal values of V_θ/V_∞ with the line joining the end points of the inlet and exit relative velocity vectors. However, since each blade has both physical thickness and a boundary layer, both of which act to reduce the flow area, the internal meridional velocity component must increase because of blockage. The mean streamline method of blade design requires that a guess be made, at this point, of the magnitude of the incremental change in V_m/V_∞ within the blade passage due to these factors. This permits construction of a curved line above the portion of the velocity diagram already constructed whose shape and level reflect the estimated change in the meridional velocity component. The points of intersection of this curved line with the vertical lines denoting the internal V_θ/V_∞ values then locate the end points of the relative velocity vectors as shown in figure 11. These relative velocity vectors thus denote the estimated magnitude and direction of the relative velocity at points on the cylindrical section corresponding to $0.0l$, $0.2l$, $0.4l$, $0.6l$, $0.8l$, and $1.0l$. The estimated increments in V_m/V_∞ at $0.0l$ and at $1.0l$ are due to the fact that the actual blade surface extends slightly forward of the $0.0l$ line and to the fact that the boundary-layer displacement thickness represents blockage at $1.0l$. Identical reasoning applied to the stator cylindrical section at $r/r_B=0.265$ permits construction of the relative velocity diagram shown on the left in figure 12. Note that in figures 11 and 12 the basic construction is made over a background of horizontal lines that subdivide l into 10 equal increments.

The mean streamline development is initiated by constructing a continuous line made up of segments extending from $0.0l$ to $0.1l$, $0.1l$ to $0.3l$, $0.3l$ to $0.5l$, $0.5l$ to $0.7l$, $0.7l$ to $0.9l$, and $0.9l$ to $1.0l$, respectively. The line segment extending from $0.0l$ to $0.1l$ is constructed parallel to the $0.0l$ relative velocity vector. The next segment in this line is then drawn, in the region from $0.1l$ to $0.3l$, by constructing a line segment parallel to the $0.2l$ relative velocity vector. The remaining segments are constructed by repeated application of this process and the mean streamline is developed by passing a spline curve through the points on this line at $0.0l$, $0.2l$, $0.4l$, $0.6l$, $0.8l$, and $1.0l$.

The blade cylindrical section is then specified by definition of the blade chord, the blade camber line, and the blade maximum thickness and thickness distribution. The steps required in this development are as follows:

(1) The approximate length of the blade chord is given by the length of the straight line that joins the points where the mean streamline intersects the $0.0l$ and $1.0l$ lines.

(2) The blade camber line is displaced from the mean streamline and is constructed by

(a) Determining the maximum value of the departure of the camber line from the mean streamline, $(\Delta n)_{\max}$, by use of equation (30).

$$(\Delta n)_{\max} = \left(\frac{\Delta n_1}{C}\right)_{\max} C\, C_L \tag{30}$$

In equation (30), $(\Delta n_1/C)_{\max}$, the maximum value of the ratio of the camber line departure from the mean streamline for unit lift coefficient to the chord length, is given in reference 14 as a function of β_V the vane chord angle measured from the axial direction. The lift coefficient is given by equation (31) where t, the blade-to-blade spacing, is given by $2\pi r/N$.

$$C_L = 2\,\frac{V_\theta}{W_m}\,\frac{t}{C} \tag{31}$$

(b) Determining the variation of the departure of the camber line from the mean streamline as a function of position along the blade chord. In reference 14, the variation of $\Delta n/(\Delta n)_{\max}$ with distance from the blade leading edge in percent chord length is given as a function of the type of blade loading distribution. The values of $\Delta n/(\Delta n)_{\max}$ presented in table II have been used in recent propulsor designs at the Ordnance Research Laboratory. These values are identical to those presented in reference 14 except in the leading edge region where the magnitudes have been reduced in an attempt to reduce the susceptibility to leading edge suction face cavitation. Multiplication of these ratios by $(\Delta n)_{\max}$ as calculated above defines the variation of Δn with distance along the chord.

(c) Constructing lines perpendicular to the chord line at the chordwise points where Δn has been evaluated. Points on the camber line are then defined by locating points on these perpendiculars that are Δn units from the mean streamline. The camber line is then defined by passing a spline curve through these points.

(3) The blade thickness is distributed symmetrically about the camber line. The thickness is determined by the product of the ratios $(T/T_{\max})\,(T_{\max}/C)$ where $T/T_{\max}$ is expressed as a function of distance from the blade leading edge in percent chord length and $T_{\max}/C$ expresses the ratio of the maximum thickness to the chord length. Recent Ordnance

Research Laboratory designs have been based on the T/T_{max} distribution listed in table III and $T_{max}/C = 0.065$. Specification of the blade cylindrical section is completed by (1) constructing lines perpendicular to the camber line at the chordwise points where the blade thickness has been defined, (2) defining points on the blade surface by locating points on these perpendiculars that are $T/2$ units on either side of the camber line, and (3) defining the blade contour by matching the end points of spline curves passed through these blade surface points to elliptical sections drawn symmetrically about the camber line end points.

TABLE II.—*Deviation of Camber Line from Mean Streamline*

Percent chord	$\Delta\eta/(\Delta\eta)_{max}$
0	0.125
10	0.510
20	0.770
30	1.025
40	1.200
50	1.370
60	1.500
70	1.540
80	1.420
90	0.970
100	0

TABLE III.—*Blade Thickness Distribution*

Percent chord	T/T_{max}
0	0
3	0.271
10	0.411
20	0.583
30	0.740
40	0.878
50	0.967
60	0.999
70	0.954
80	0.796
90	0.519
99	0.194
100	0

The blade section defined by this process represents a first approximation only since its construction was based on an estimate of the internal changes in V_m due to blockage and since the length of the chord was approximated by the length of the line joining the end points of the mean streamline. The chord length is defined as the length of the line that connects the end points of the camber line.

A second application of the mean streamline method of blade design should be made at this point. In this application, the internal changes in V_m can be calculated by utilizing values of the blade thickness measured normal to the meridional direction, taken from the initial approximation of the blade cylindrical section, and estimated values of the boundary-layer displacement thickness. In addition, the blade chord can be constructed by applying the value of Δn calculated for the zero-percent chord position in the initial approximation at the point where the revised mean streamline intersects the $0.0l$ line to locate the approximate true end point for the revised chord.

The calculation of the blockage correction to the meridional velocity is based on the following reasoning. As the flow proceeds through the blade passages, the meridional velocity is affected by blockage due to the blade thickness and to the boundary-layer displacement thickness. Thus, to satisfy the continuity equation, the local meridional velocity must increase above the base value which would exist in the absence of these factors. Base values of the meridional velocity for the Akron blade sections were obtained by assuming a linear variation of V_m with l' as indicated in figures 11 and 12. If the local base value of the meridional velocity is designated as $V_{ml'}$, then reference to figure 13 permits definition of the required correction $\Delta V_{ml'}$. Considering a cylindrical section of height Δr, the continuity equation becomes

$$\rho V_{ml'} t(\Delta r) = \rho(V_{ml'} + \Delta V_{ml'})(t-\tau)(\Delta r) \tag{32}$$

which reduces to

$$\frac{\Delta V_{ml'}}{V_\infty} = \frac{V_{ml'}}{V_\infty} \frac{\tau}{t-\tau} \tag{33}$$

where τ is the sum of the local blade thickness, measured normal to the meridional direction, and the total local boundary-layer displacement thickness. A rational estimate of the displacement thickness can be obtained by the method outlined in reference 16. This method requires the selection of a skin friction factor and a form factor representative of a turbulent boundary layer that has been subjected to an adverse pressure gradient.

Past experience has shown that two applications of the mean streamline method of blade design are generally sufficient. Exceptions have been

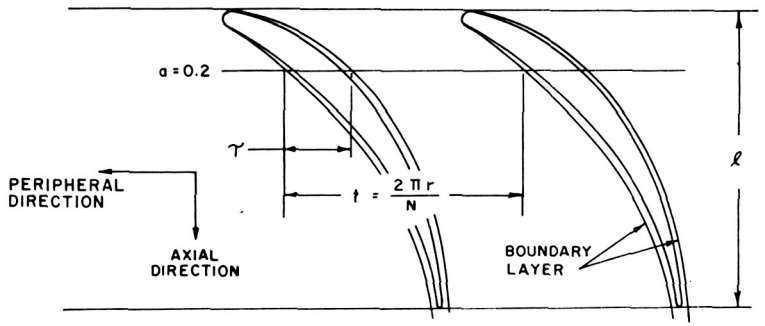

FIGURE 13.—*Cylindrical section development illustrating meridional flow blockage.*

noted in cases where a particularly poor initial guess of the blockage effects has been made; however, it is safe to say that this iterative design procedure converges very rapidly. The blade sections shown in figures 11 and 12 are based on three applications of the design method. For these sections, the differences between the blade profiles obtained in the second and third approximations were negligible.

The blade section pressure distributions shown in figures 11 and 12 were determined by (1) calculating the variation of the mean pressure, $p_{l'}$, with position along the axial length and (2) constructing the blade pressure diagram about the mean pressure line by dividing the $\Delta p/(\frac{1}{2}\rho V_\infty^2)$ distributions shown on the right in figures 11 and 12 between the suction and pressure sides of the blades in a two-thirds/one-third distribution.

The mean pressure variation was found by writing Bernoulli's equation to relate flow conditions on a streamline at the inlet to flow conditions at the point where the streamline crosses the blade cylindrical section. For the rotor, if the subscripts 2 and l' refer to points at the inlet and on l, then

$$p_2+\tfrac{1}{2}\rho V_{m_2}^2=p_{l'}+\tfrac{1}{2}\rho V_{m_{l'}}^2+\tfrac{1}{2}\rho V_{\theta_{l'}}^2-\frac{l'}{l}\,(\Delta P_T)-\rho U V_{\theta_{l'}}$$

where ΔP_T represents the difference in total pressure at the inlet between streamlines that intersect l at $l'=0$ and at $l'=l$, and $\rho U V_{\theta_{l'}}$ represents the pressure increment associated with development of the rotor head H.

Nondimensionalizing these relations by the factor $\frac{1}{2}\rho V_\infty^2$ leads to equation (34) which is the desired form for the variation of the mean static pressure as a function of l' for rotor blade cylindrical sections.

$$\frac{p_{l'}-p_2}{\frac{1}{2}\rho V_\infty^2}=\left(\frac{V_{m_2}}{V_\infty}\right)^2-\left(\frac{V_{m_{l'}}}{V_\infty}\right)^2-\left(\frac{V_{\theta_{l'}}}{V_\infty}\right)^2+\frac{l'}{l}\,\frac{\Delta P_T}{\frac{1}{2}\rho V_\infty^2}+2\,\frac{U}{V_\infty}\,\frac{V_{\theta_{l'}}}{V_\infty} \qquad (34)$$

Equation (35) was derived on the basis of similar reasoning and represents the variation

$$\frac{p_{l'}-p_4}{\frac{1}{2}\rho V_\infty^2}=\left(\frac{V_{m_4}}{V_\infty}\right)^2+\left(\frac{V_{\theta_4}}{V_\infty}\right)^2-\left(\frac{V_{m_{l'}}}{V_\infty}\right)^2-\left(\frac{V_{\theta_{l'}}}{V_\infty}\right)^2+\frac{l'}{l}\frac{\Delta P_T}{\frac{1}{2}\rho V_\infty^2} \tag{35}$$

of the mean static pressure with l' for stator blades.

The basis for the two-thirds/one-third distribution of the static pressure change between the suction and pressure sides of the blade is empirical and is based on examination of the NACA cascade test results. An experimental cascade program is in progress at the Ordnance Research Laboratory at present, one of whose objectives is a critical evaluation of available theoretical and empirical blade design methods. A summary of this program is presented in Appendix II. Results from this program will be used as they become available to verify and/or modify the mean streamline method of blade design.

Values of the cavitation index σ and of the diffusion factor D, defined by equation (15) with $p_V=p_{\min}$, and by equation (24), respectively, are presented in the following table for the rotor and stator blade sections. These values are well below the maximum design values, $\sigma=0.650$ and $D=0.500$.

Blade Section	σ	D
Rotor at $r/r_B=0.345$	0.244	0.273
Stator at $r/r_B=0.265$	0.314	0.304

The design of individual cylindrical blade sections for the rotor and stator of the Akron pumpjet has been described in detail. An adequate design of the rotor and stator blading would require the design of additional cylindrical sections at values of r/r_B both above and below the values selected here for illustrative purposes.

LIST OF SYMBOLS

A	Area
A_B	Frontal area of body
A_s	Wetted surface area
a	Fractional portion of projected chord length
C_{D_S}	Shroud frictional drag coefficient based on body frontal area
C'_{D_S}	Shroud frictional drag coefficient based on shroud wetted surface area
C_T	Thrust coefficient
$C_{D_{BB}}$	Bare-body drag coefficient
C_b	Blade pressure coefficient

C_P	Power coefficient
C_m	Mass flow coefficient
C_L	Lift coefficient
C	Chord length
D_B	Maximum body diameter
D	Diffusion factor
g	Gravitational constant
H	Head (fluid energy)
H_R	Head (shaft energy)
h_{sub}	Submergence depth in feet
h_{atm}	Atmospheric head in feet
J	Advance ratio
K	Inlet loss coefficient
K_{aR}	Rotor load distribution factor
K_{aS}	Stator load distribution factor
l	Projected length of chord in peripheral direction
l'	Fractional distance of l defined by $l' = al$
l_s	Shroud chord length
N	Number of blades
n	Rotor shaft speed
$(\Delta n)_{\max}$	Maximum departure of camber line from mean streamline (normal to chord)
P_T	Total pressure
p	Static pressure
r	Local radius
r_B	Maximum body radius
r_T	Tip radius
r_H	Hub radius
$r_{3l'}$	Radial position at rotor trailing edge of the streamline that passes through the rotor cylindrical section at l'
$r_{4l'}$	Radial position at stator leading edge of the streamline that passes through the stator cylindrical section at l'
r_{ψ_1}	Radial location of stagnation streamline at Station ①
T	Blade thickness normal to camber line
t	Blade pitch, defined as $t = 2\pi r/N$
U	Peripheral blade velocity
V	Absolute velocity
W	Relative velocity
W_m	Mean relative velocity
β_v	Vane angle between chord line and axial direction
γ	Volumetric density
θ	Angle between meridional and axial direction
η_H	Hydraulic efficiency
ρ	Mass density

σ	Cavitation index
ω	Angular velocity
Δ	Incremental difference

Subscripts

1, 2, 3, 4, 5, 6, 7	Flow stations of figure 2
a	Axial component
m	Meridional component
θ	Peripheral component
∞	Ambient free-stream conditions

Superscripts

$-$	Average value of quantity based on mass flow rate
$=$	Average value of quantity based on momentum
$\sim$	Average value of quantity based on energy

APPENDIX I. Computerized Streamline Curvature Method

The indirect turbomachine design problem entails the specification of a blade geometry to produce a set of desired performance characteristics. Within the limits of the current development, the solution of the indirect problem requires the determination of the inlet and exit velocity profiles produced by a specified peripheral velocity distribution at the blade boundary planes and any associated variation in total pressure through the blade passage.

Simple radial equilibrium theory has often been used to gain a first approximation of the velocity distributions; however, this method neglects the effects of the meridional curvature of the streamlines and is rather limited in the variety of situations to which it is applicable. When the effects of the meridional radius of curvature are included in the radial equilibrium equation, the calculation process is termed the streamline curvature method. Smith, Traugott, and Wislicenus in reference 19 presented a detailed analysis which included these streamline curvature effects.

Historically, attempts to accurately employ the streamline curvature method have been hampered by the necessity of physically measuring the geometric input data and by the tedious iterations required for a solution. The current development of the streamline curvature method as an accurate design procedure has been made possible by the use of digital computers to perform the iteration processes and by the advent of the so-called spline functions (ref. 20) for data specification.

The spline function is a mathematical model of a thin elastic beam used to represent a draftsman's plastic spline. The importance of the spline function is its ability to accurately produce valid and continuous values of a function, and of its first and second derivatives. Thus, by employing spline functions to specify the flow parameters and stream patterns, it is no longer necessary to rely on physical measurements of slopes and radii of curvature. These properties can be calculated directly from the spline functions.

The current development of the computerized solution of the indirect axisymmetric turbomachine problem by the streamline curvature method relied heavily on the work of Novak in reference 21. A detailed development of the basic equations of motion and of the computer program (SCM I) is presented in reference 15, where the problem to be solved is stated as follows: Given the geometry of the flow boundaries, the reference pressure and velocity profiles, and the desired blade performance (i.e., the peripheral velocity distribution at the blade exit planes), determine the streamline pattern and the associated pressure and velocity distributions for the axisymmetric flow through the blade system.

Essentially, the program computes an iterative solution using the cylindrical form of the equations interrelating (1) continuity, (2) conservation of angular momentum, (3) constant total pressure along a streamline in the absence of any energy sources, and (4) radial equilibrium. The following assumptions have also been included in the analysis:

(1) The flow is axisymmetric and free of secondary flows.
(2) The fluid is inviscid and incompressible.
(3) The flow processes occur under steady-state conditions and at a constant temperature.
(4) All pressure losses along the streamlines are neglected.

A typical flow field to be analyzed is illustrated by the geometry in figure 2, where the velocity and pressure distributions at Station ① are assumed to be known from experimental or theoretical data and where the peripheral velocity distributions at the exit planes of the rotor and stator have been specified. The axial station locations are chosen so that they accurately describe the geometry of the flow field and are in locations of desired data output.

Spline curves are passed through the input data as a function of radial distance at the appropriate stations. At the reference station, Station ① the streamline location is derived based on equal increments of mass flow rate coefficient between streamlines. The first approximation of the streamline pattern at the remaining stations is formed in proportion to the flow area at the respective station. Spline curves are passed through this streamline pattern and the necessary geometric properties are calculated. The total pressure coefficient is specified as a constant along a

given streamline from the reference station to the rotor inlet; at the rotor exit the total pressure is incremented by the rotor head and specified as a constant at the new value for the remaining stations.

The appropriate equations and required data from the spline curves are employed to determine the meridional velocity profiles for all stations other than the reference station. This entails an iteration process between the assumed value of meridional velocity at the midstreamline and the continuity equation. These newly formed profiles are integrated to determine a new streamline pattern which is then adjusted according to the procedure suggested by Horlock in reference 22. Spline curves are then developed to define these new streamline shapes as a function of axial position. The entire process is repeated until the difference in streamline location for two successive passes through the program is within a specified limit for all streamlines at all stations. When this static condition is reached, the program has defined the final solution.

The program then enters the output phase. Geometrically, the output data at each station may be specified along a line at any specified angle with respect to the centerline. At each station the program outputs the x and y coordinates of the streamline pattern and the corresponding values of meridional velocity ratio, peripheral velocity ratio, static pressure coefficient, total pressure coefficient, local flow angle, and the meridional radius of curvature of the streamline. Also included in the output are the evaluations of the mean rotor head and torque coefficient.

The results of the program have agreed very well with alternate axisymmetric solutions such as the graphical technique described by Gearhart in reference 23. In general, the agreement between experimental data and that presented by the SCM I computer program is good; the differences are thought to result from real fluid effects not included in this perfect fluid solution. It is planned to incorporate an empirical estimate of the streamwise and spanwise energy losses in the near future.

APPENDIX II. ORL Cascade Research Program

Success in performing fundamental turbomachinery research using the subsonic cascade tunnel as the basic experimental tool is exemplified by the results of the research effort at the University of Liverpool which are summarized in reference 24.

With a subsonic porous wall tunnel not only can two-dimensional flow be obtained, but the capability of varying the axial velocity ratio exists and it is possible to obtain cascade performance data over a range of axial velocity ratios. With such capability, the blade boundary-layer growth and secondary flows can be modeled and studied in detail. Blade end wall losses and blade separation limits can also be established. Efforts at the

Ordnance Research Laboratory directed toward the development of hydrodynamic blading having surface velocities of minimum magnitude near the blade leading edge, thereby providing maximum resistance to cavitation, have required the design, fabrication, and operation of a cascade flow facility as shown by figures 14 and 15.

The initial tests in this facility are being directed toward clarifying two problems which remain regarding the application of the mean streamline method of design.

(1) A risk is encountered when using trailing edge loaded blades which create steep, adverse pressure gradients near the trailing edge. The degree of adversity of a pressure gradient can only be decided by cascade tests which can show whether a design load distribution over a blade is satisfactory or unsatisfactory. Use of a trailing edge loaded blade implies that an adverse pressure gradient on the forward portion of the blade has been intentionally reduced to provide increased cavitation resistance while the pressure gradient at the aft end has been made more adverse to permit carrying the same total load as a forward loaded blade. Concerning blade losses (not cavitation resistance), the NACA has developed trailing edge loaded profiles of acceptable performance as reported in reference 25. In a similar manner, through cascade tests, the Ordnance Research Laboratory must produce similar performance curves for their profiles which have different thickness and loading distributions.

(2) The mean streamline method of design, reference 14, is semi-empirical in that the deviation of the blade camber line from the mean streamline is based on offsets derived from existing NACA cascade data. Generating similar cascade data for blading having an extended range of

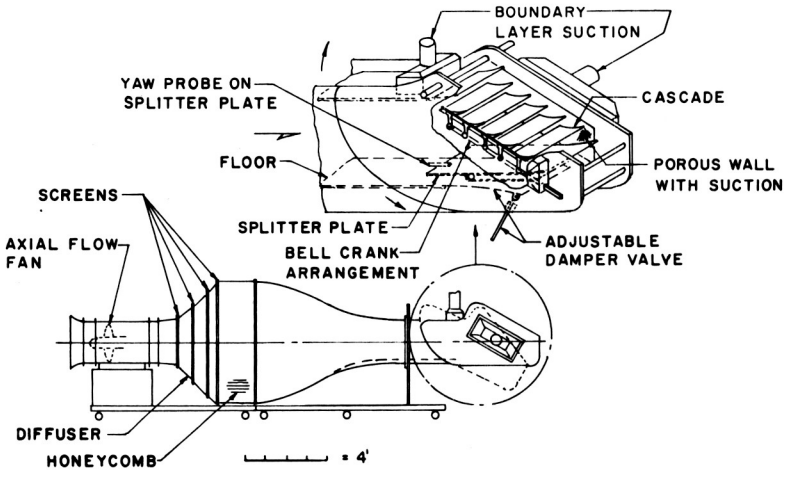

FIGURE 14.—*Schematic of subsonic cascade tunnel.*

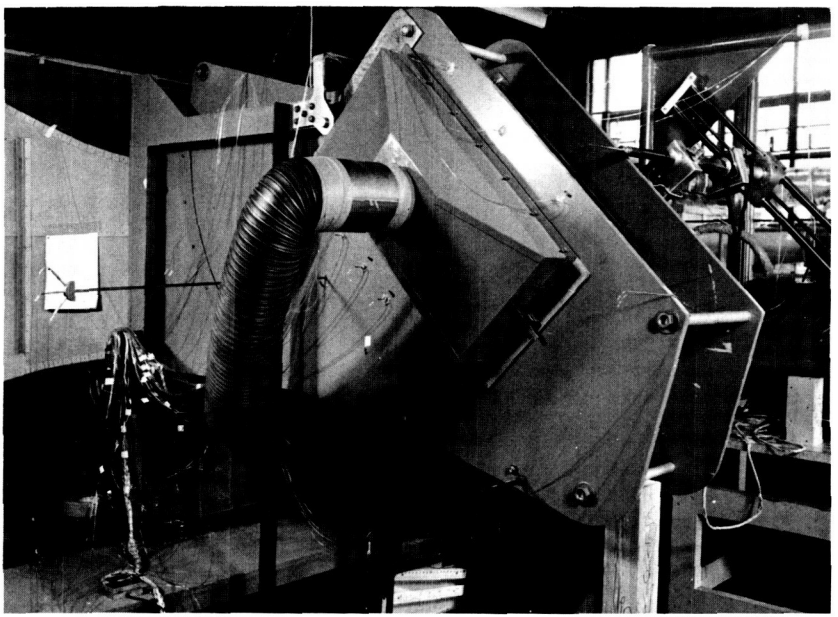

FIGURE 15.—*Test section of cascade tunnel.*

solidities ($c/t > 1.5$), and with alternate thickness and loading distributions will further strengthen an already proven design method.

On this basis, a series of two-dimensional blade geometries utilizing the table III thickness distribution and the loading distributions of figures 11 and 12 have been designed and fabricated to permit an experimental evaluation of their pressure distributions and loss characteristics. Concurrently, a theoretical analysis of these cascade geometries is being conducted. Successful prediction of the pressure distribution of the tested blade geometries using the theoretical analysis will permit many geometries to be analyzed theoretically with only periodic experimental verification to ensure that the limitations of the potential solution have not been exceeded.

The theoretical solution selected for use in this program is outlined in reference 26. This reference also lists the computer program for use on an IBM 7090. The terminology in the reference is somewhat different from that commonly used in NACA compressor cascade reports. The program has been rewritten for use on the IBM 360 digital computer and the geometry of the cascade has been redefined in the more common cascade terminology. Application of this analysis to various cascade geometries and a listing of the program for use on the IBM 360 digital computer is given in reference 27. In this reference, it is shown that the comparison

between the pressure diagrams obtained analytically and those obtained experimentally by the NACA for the same cascade geometries is quite good, even for blades operating far from zero incidence. As might be expected, the analytical solution predicts more turning of the flow than is obtained experimentally. This difference is thought to be due to viscous effects which are neglected in the analytical solution.

An effort has been initiated which will permit including real fluid effects in the potential solution. The revised method will require using the potential flow pressure distribution to obtain the boundary-layer displacement thickness along the pressure and suction surfaces of the blade. This thickness will then be added to the blade thickness and the resulting cascade geometry will be reinserted in the Douglas Neumann program of reference 27 to obtain corrected fluid deflection data.

The experimental results which have been obtained from the cascade program to date are reported in reference 28. A summary is also presented in this reference of the test procedures, operating characteristics, and capabilities of the cascade test facility.

REFERENCES

1. Brandau, John H., *Aspects of Performance Evaluation of Waterjet Propulsion Systems and a Critical Review of the State-of-the-Art.* NSRDC Report 2550, October 1967.
2. Gearhart, W. S., and R. E. Henderson, Selection of a Propulsor for a Submersible System. *J. Aircraft*, Vol. 3, No. 1, January-February 1966.
3. Wislicenus, G. F., and L. R. Smith, *Hydraulic Jet Propulsion and Incipient Cavitation.* Internal Flow Research Report I-6, Part A, Johns Hopkins U. Mech. Eng. Dept., March 21, 1952.
4. Brooks, J. D., and T. G. Lang, Simplified Methods for Estimating Torpedo Drag. *Underwater Missile Propulsion*, L. Greiner, ed., Compass Publications, Inc. (Arlington, Virginia), 1967, pp. 117–146.
5. Mayer, A., and F. J. Hill, *On a Rapid Estimate of Inlet Velocity Distribution for a Pumpjet Operating in a Prediffused Turbulent Boundary Layer of an Axially Symmetric Body.* NOTS Report TM 671.
6. Freeman, *H. B., Measurements of Flow in the Boundary Layer of a 1/40 Scale Model of the U.S. Airship Akron.* NACA Report No. 430, 1932.
7. Wislicenus, G. F., Hydrodynamics and Propulsion of Submerged Bodies. *J. Am. Rocket Soc.*, Vol. 30, 1960, pp. 1140–1148.
8. Thurston, S., and M. S. Evanbar, *The Efficiency of a Propulsor on a Body of Revolution Inducting Boundary Layer Fluid.* AIAA Paper No. 65–234, presented at the Marine Systems and ASW Conference (San Diego), March 1965.
9. Schlichting, H., Application of Boundary Layer Theory in Turbomachinery. *Trans. ASME, J. Basic Eng.*, Series D, Vol. 81, 1959, pp. 543–551.
10. Eskinazi, S. J., C. D. Flagle, J. R. Ruetenik, and J. R. Weske, *A Problem in Retardation of a Turbulent Boundary Layer.* Inst. Cooperative Res., Johns Hopkins U., Report I–6, Part B, March 1952.
11. Rains, D. A., *Tip Clearance Flows in Axial Flow Compressors and Pumps.* Cal. Tech., Report 5, June 1954.

12. MITCHELL, A. B., *An Experimental Investigation of Cavitation Inception in the Rotor Blade Tip Region of an Axial Flow Pump.* ARL Report ARL/R1/G/HY/11/2, August 1958.
13. GEARHART, W. S., Tip Clearance Cavitation in Shrouded Underwater Propulsors. *J. Aircraft*, Vol. 3, No. 2, March–April 1966.
14. WISLICENUS, G. F., *Fluid Mechanics of Turbomachinery*, Volumes 1 and 2. Dover Publications, Inc. (New York), 1965.
15. TREASTER, A. L., *Computerized Application of the Streamline Curvature Method to the Indirect, Axisymmetric Turbomachine Problem.* ORL TM 514.2491–16, October 31, 1969.
16. HENDERSON, R. E., J. F. MCMAHON, AND G. F. WISLICENUS, A Method for the Design of Pumpjets. *Underwater Missile Propulsion*, L. Greiner, ed., Compass Publications, Inc. (Arlington, Virginia), 1967, pp. 117–146.
17. LIEBLEIN, S., F. C. SCHWENK, AND R. L. BRODERICK, *Diffusion Factor for Estimating Losses and Limiting Blade Loading in Axial Flow-Compressor Blade Elements.* NACA RM53D01, June 1953.
18. SMITH, L. H., *Three Dimensional Flow in Axial-Flow Turbomachinery*, Parts I and II. Reports I–14 and I–16, Inst. Cooperative Res., Mech., Eng. Dept., Johns Hopkins U., November 1953.
19. SMITH, L. H., S. C. TRAUGOTT, AND G. F. WISLICENUS, A Practical Solution of a Three-Dimensional Flow Problem of Axial-Flow Turbomachinery. *Trans. ASME*, Vol. 75, No. 5, July 1953.
20. DAVIS, R. F., *Spline Curve Fit Functions, Their Derivation and Use.* ORL TM 512.3531–02, July 23, 1968.
21. NOVAK, R. A., *Streamline Curvature Computing Procedures for Fluid Flow Problems.* ASME Paper 66–WA/GT–3, November 27, 1966.
22. HORLOCK, J. H., *Axial Flow Turbines.* Butterworth Scientific Publications (London), 1966.
23. GEARHART, W. S., *Graphical Analysis of Incompressible Axisymmetric Flow.* ASME Symposium on Pumping Machinery for Marine Propulsion (Philadelphia), May 6, 1968.
24. HORLOCK, J. H., Some Recent Research in Turbo-Machinery. *Proc. Inst. Mech. Engrs.*, Vol. 182, Part I, No. 26, 1967–68.
25. ERWIN, J. R., M. SAVAGE, AND J. C. EMERY, *Two-Dimensional Low-Speed Cascade Investigation of NACA Compressor Blade Sections Having a Systematic Variation in Mean-Line Loading.* NACA TN 3817, November 1956.
26. GIESING, J. P., *Extension of the Douglas Neumann Program to Problems of Lifting Infinite Cascades.* U.S. Department of Commerce Report No. LB31653, AD605207, Revised July 2, 1964.
27. ROSS, J. R., AND L. E. ESKAY, *The Application of the Douglas Neumann Computer Program to the Analysis of Blade Cascade Geometries.* ORL TM 506.2491–31, January 31, 1969.
28. GEARHART, W. S., AND J. R. ROSS, *A Subsonic Cascade Test Facility, an Aid to Hydrodynamic Blade Design.* ORL TM 506–02, March 13, 1970.

DISCUSSION

L. MEYERHOFF (Eastern Research): Obtaining a ducted propeller design for operation in a boundary layer at the rear of a body is a difficult task. It is a nonpotential (rotational) problem, often approximated in the literature without substantive justification by a combination of potential and nonpotential methods. In the broad sense, it is necessary to contend with the effects of radially varying boundary-layer velocities, body shape, duct shape, and propulsor-body-flow interaction. To this is added the additional complication of obtaining cavitation delay for the blading and duct surfaces.

The authors present a rational approach to the problem, showing the important techniques they have developed. The discussion which follows relates mainly to the first part of the authors' paper, on the initial performance study, and, in particular, to the problem of determining where the inflow station ahead of the propulsor is to be located.

The initial performance study begins with the flow picture shown in figure 2. Here, the upstream inflow station (Station ①) is seen, as well as the propulsor which adds a total pressure rise to the flow and, finally, the issuing jet at Station ⑦. In general, all flow quantities at all stations will be radially varying. The significance of the inflow station is that its location determines the initial velocity and static pressure profiles needed for calculating both the overall propulsion design parameters and the final flow field.

It would seem that the inflow station should be defined as the first axial location ahead of the propulsor where the bare-body flow is not affected by the propulsor operation. Aft of this location, the mutual interaction of body and propulsor flows will alter the bare-body flow. Clearly, it is a difficult analytical problem to determine such a location.

How important are these considerations from the viewpoint of a practical initial performance prediction? Some preliminary information on this question follows.

In the authors' paper, the inflow is taken at a location about 82 percent back from the body nose; at this station, the bare-body static pressure coefficient is zero. Boundary-layer velocities are given in reference 6 of the authors' paper.

Eastern Research Group (ERG) has obtained corresponding performance results using three other nearby inflow stations which bracket the authors' 82-percent location.

Figure D–1 shows these velocity profiles of reference 6 at 67.9-percent, 77.5-percent, and 86.9-percent axial body stations; body static pressure coefficients at these stations are about $-.075$, $-.025$, and $+.030$, respectively.

These flow velocities were inserted as input data for a computer program developed at ERG. Since the radial variation of static pressure at the inflow stations is not available in reference 6, this will be taken as radially constant but at one-half the values given previously. (The authors take a zero value.)

The thrust equation used by ERG is

$$\text{Thrust} = \int (V_7 - V_1 \cos\theta)\, d(\text{mass flow}) - \int (p_1 - p_7)\, dA_1$$

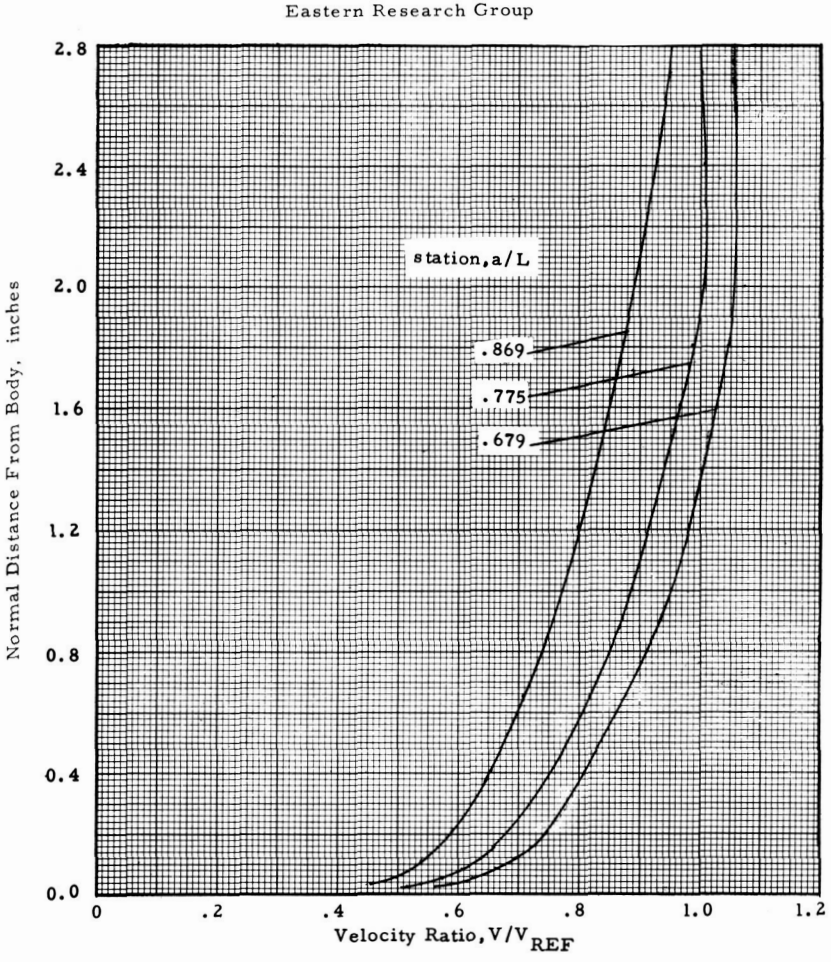

FIGURE D–1.—*Akron boundary-layer profiles.*

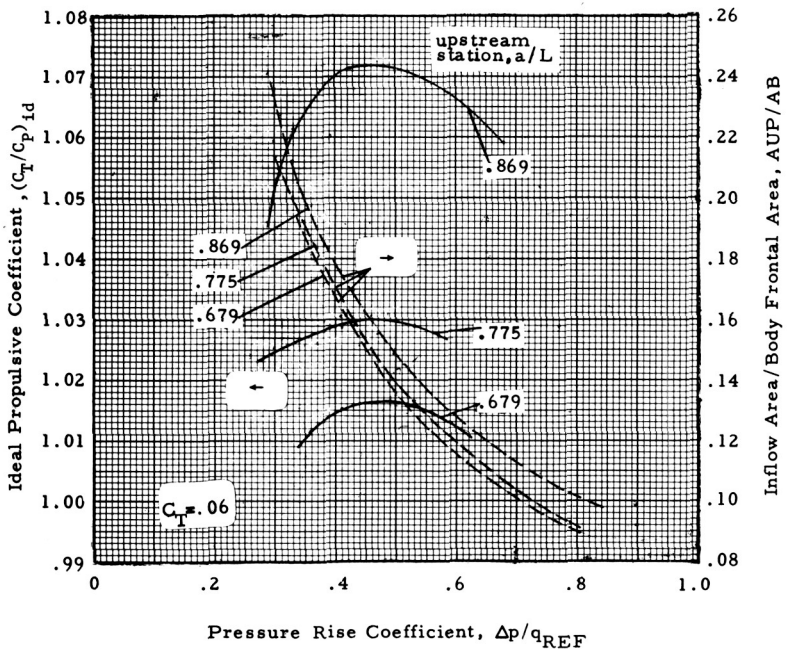

FIGURE D–2.—*Ideal efficiency and inflow area versus required propulsor pressure rise.*

where p_7 is assumed to be the static ambient value at the body centerline. The need for the static pressure term is avoided in the authors' paper by choosing an inflow station where the pressure is ambient and assuming, as in the ERG equation, that the jet static pressure is at the ambient value.

Figure D–2 shows the effect of inflow station location on ideal efficiency[D-1] defined by $(C_T/C_p)_{id}$ and inflow area ratio A_1/A_B. This ideal efficiency does not contain blading efficiency or duct inflow loss. The thrust coefficient is $C_T = .06$. The abscissa of figure D–2 is the total pressure rise coefficient needed to produce $C_T = .06$, and is taken as radially constant; q_{REF} is the free-stream dynamic pressure. Efficiencies are seen to progressively increase as the inflow station is moved back from the body nose. A maximum 6-percent difference is seen between the 67.9-percent and 86.9-percent stations. The total pressure rise required at maximum

[D-1] Propulsive coefficient (P.C.) is generally defined as RV/power; where R is bare-body resistance, V is vehicle speed, and power is that delivered to the rotor. The relation between P.C. and the ideal efficiency $(C_T/C_P)_{id}$ of figure D–2 is P.C. = $(C_T/C_P)_{id}\ (1 - t)\eta$, where η is the conventional blading efficiency and $1 - t$ is the naval architect's thrust factor; i.e., required net thrust equals [bare-body resistance/$(1 - t)$] + duct drag (with rotor operating). The authors' paper assumes $t \sim 0$; see the sixth paragraph of the section on optimum propulsor mass flow.

efficiency appears to be independent of inflow location. Inflow area ratios, A_1/A_B, shown in figure D–2 are seen to increase with distance back along the body.

Figure D–3 shows the effect of inflow station on the local velocity ratio at the stagnation line radius of Station ① (fig. 2 of authors' paper). This velocity is seen to change significantly with inflow station location. The differences in velocity ratios in figure D–3 can be of importance for rotor blade cavitation inception.

Figure D–4 shows the jet radius and mass flow coefficient corresponding to the data in figure D–2 and D–3. The jet radius appears to be independent of inflow station location and this may be peculiar to the body velocity profiles used. It is interesting to observe that the jet radius is

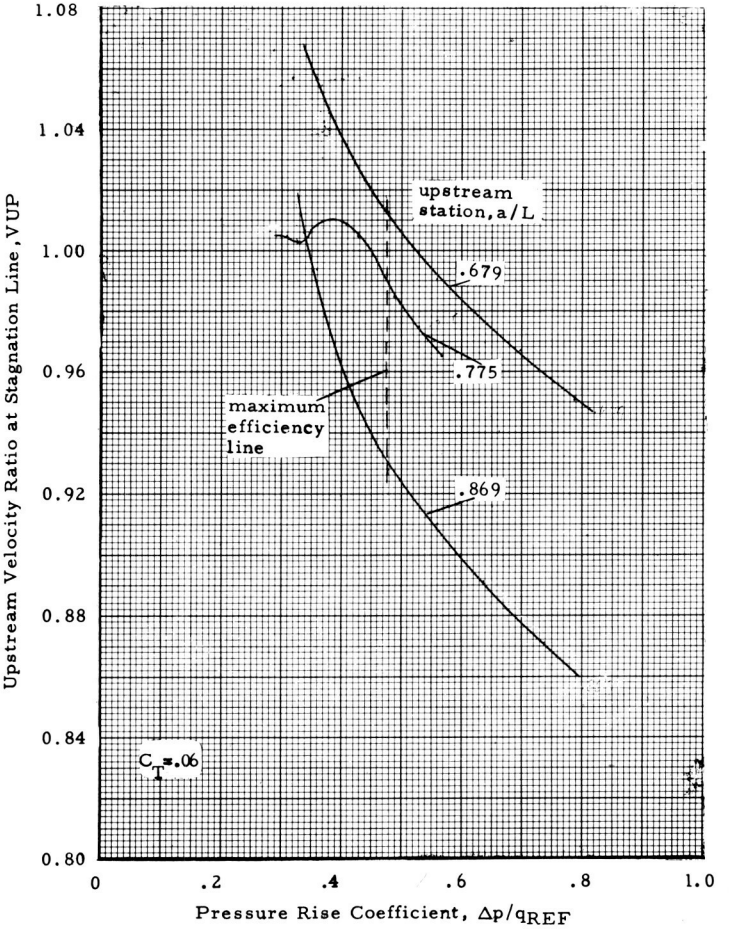

FIGURE D–3.—*Velocity ratio at upstream stagnation-line radius.*

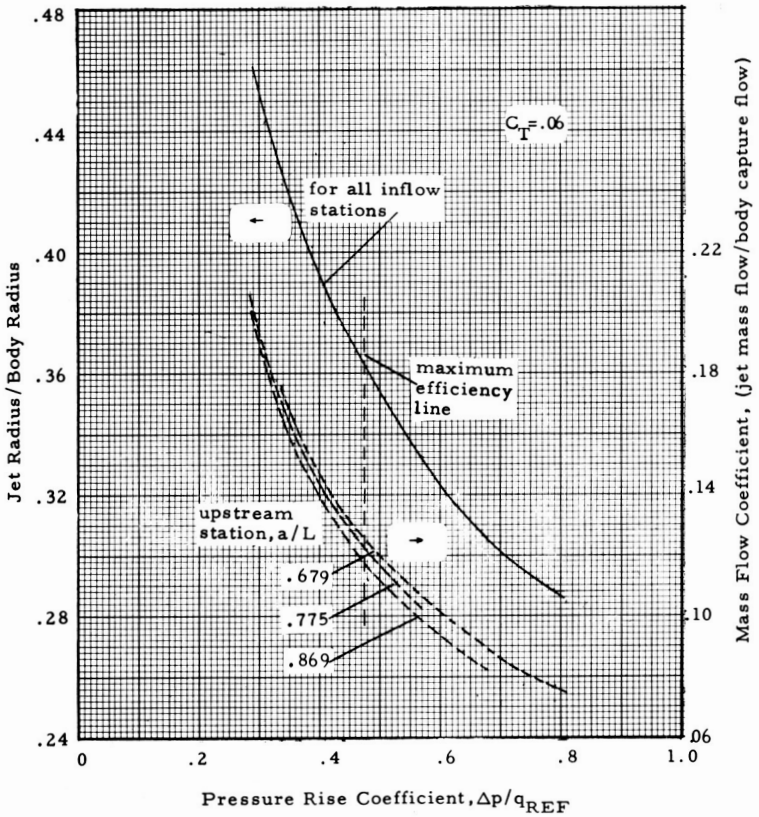

FIGURE D–4.–*Jet radius and mass flow.*

about 36 percent of the maximum body radius for peak ideal efficiency. Mass flow changes in figure D–4 are seen to have a relatively small change with inflow station.

It can be concluded that the selection of the inflow location may have a significant effect. The choice of the inflow location appears to affect the efficiency, upstream velocity, and inflow streamtube area. Still unresolved is the effect of inflow station on the detailed flow field.

Finally, there appear to be differences in results between the averaged flow method of the authors' paper and the direct integration approach as used by ERG. At the maximum efficiency point for the 82-percent station, these differences are

(1) Inflow area ratio is about 0.12 (fig. 3) versus 0.19 in figure D–2.

(2) Stagnation line velocity at ① is about 0.90 (figs. 1 and 3) versus 0.97 in figure D–3.

W. B. MORGAN (Naval Ship Research and Development Center): I have two comments. The first is in regard to the performance obtained using this procedure. How well do you predict the shaft horsepower?

The other question has to do with the optimum mass flow. I take exception to the word optimum if I understand correctly what you mean. We want to design for given speed or given cavitation characteristics and it really is not quite clear how we select the duct in the sense of its length. Also, it seems that the use of just the optimum mass flow does not properly take into consideration the drag of the duct, the induced drag about the duct, the interaction between the duct and the hull, and the interaction between the impeller and hull. These really are not all considered, and I wonder, when you talk about the optimum diameter using optimum mass flow, how close that is.

BRUCE, GEARHART, ROSS, AND TREASTER (authors): The comments of Dr. Meyerhoff with regard to the care that must be exercised in selecting the location of the upstream reference station are highly pertinent. This is particularly true if one is considering the flow to be inviscid downstream of this station. The momentum and energy relations which are subsequently utilized to predict the overall performance of the propulsor are quite dependent on the reference station flow characteristics. In addition, the induced effects of the shroud on the reference station flow characteristics must be considered. A potential solution indicates that the upstream induced flow effects from a cascade of blade profiles are negligible one chord length upstream. On this basis, the authors' practice has been to select a reference station at least one shroud length upstream of the shroud inlet.

In the paper, the drag coefficient was not held constant as ingested mass flow changed, but was varied in a manner that reflected the inlet losses and the added frictional drag on the shroud. This is felt to be more realistic than the approach used in the analysis of the discussor and could account, to some degree, for the deviations in the results. From Dr. Meyerhoff's analysis, he reaches the conclusion that neither rotor total pressure rise nor pumpjet mass flow varies with choice of reference station, which implies that required shaft power does not depend on choice of reference station. This effect is felt to be artificial due to the fact that shroud drag was held constant in his calculations.

Dr. Morgan inquired about the degree of success that had been experienced in applying the design approach of the paper. A number of pumpjet propulsors have been designed over a relatively wide spectrum of advance ratios and ingested mass flow coefficients. Model tests of these units indicate that predicted and measured shaft torque at a given shaft speed can be matched within 3 to 4 percent. Cavitation performance has been found to generally exceed those values predicted by the methods outlined.

Several units have been tested which provided overall cavitation indices less than 0.5.

With regard to the comments on the method for selecting the optimum mass flow, consider a ring shroud moving forward along a line parallel to its axis of revolution and its similarity to an infinite airfoil. In steady flow there are no vortices shed since there are no circumferential changes in circulation. Therefore, there is no induced drag. In addition, the rotation in the far wake of the jet is zero and the associated pressure drag is zero since the stator system has provided an axial discharge jet. Thus the increment of added drag normally experienced by a shrouded propeller without a stator system or by a single open propeller is nonexistent when the pumpjet is considered. If the shroud is nonseparating, it is felt that a rational approximation of the shroud drag is obtained by combining the frictional losses on the wetted surface area and the energy losses at the shroud inlet. These considerations have been included in the analysis leading to the selection of the optimum mass flow, thereby minimizing the overall power coefficient of the propulsor for a given vehicle.